

DNA Damage | Very Important Paper |

VIP Metal Exchange in the Interprotein Zn^{II}-Binding Site of the Rad50 Hook Domain: Structural Insights into Cd^{II}-Induced DNA-Repair InhibitionMichał Padjasek,^[a] Maciej Maciejczyk,^[b] Michał Nowakowski,^[c] Olga Kerber,^[a] Maciej Pyrka,^[b] Wiktor Koźmiński,^[c] and Artur Krężel*^[a]

Abstract: Cd^{II} is a major genotoxic agent that readily displaces Zn^{II} in a multitude of zinc proteins, abrogates redox homeostasis, and deregulates cellular metalloproteome. To date, this displacement has been described mostly for cysteine(Cys)-rich intraprotein binding sites in certain zinc finger domains and metallothioneins. To visualize how a Zn^{II}-to-Cd^{II} swap can affect the target protein's status and thus understand the molecular basis of Cd^{II}-induced genotoxicity an intermolecular Zn^{II}-binding site from the crucial DNA repair protein Rad50 and its zinc hook domain were examined. By using a length-varied peptide base, Zn^{II}-to-Cd^{II} displacement in Rad50's hook domain is demonstrated to alter

it in a bimodal fashion: 1) Cd^{II} induces around a two-orders-of-magnitude stabilization effect ($\log K_{\text{Zn}^{\text{II}}}^{12} = 20.8$ vs. $\log K_{\text{Cd}^{\text{II}}}^{12} = 22.7$), which defines an extremely high affinity of a peptide towards a metal ion, and 2) the displacement disrupts the overall assembly of the domain, as shown by NMR spectroscopic and anisotropy decay data. Based on the results, a new model explaining the molecular mechanism of Cd^{II} genotoxicity that underlines Cd^{II}'s impact on Rad50's dimer stability and quaternary structure that could potentially result in abrogation of the major DNA damage response pathway is proposed.

Introduction

Cadmium is a well-defined nephrotoxic, pneumotoxic, osteotoxic, and cardiotoxic agent and, on top of that, a strong carcinogen, a feature probably stemming from its extensive indirect genotoxicity.^[1–5] Its detrimental effects on human health are known, but a clear mechanism connecting cadmium's intake

and its indirect genotoxicity is still elusive, which seems to be dictated by a multivalent effect occurring as a result of binding of the Cd^{II} ion by its cellular targets.^[6] Cd^{II} as a softer Lewis acid than Zn^{II} readily displaces it in cysteine(Cys)-rich zinc-binding proteins and biomolecules, which solitarily introduces an enormous toxic effect inside a cell.^[7] Zn^{II} fluctuations, which impact the exchangeable zinc quota,^[8] interfere with redox homeostasis, and deregulate cellular metalloproteome.^[9] Furthermore, because Cd^{II} binds preferentially to thiol-containing and other nucleophilic ligands, it interacts with a wide spectrum of redox signaling and reactive oxygen scavenger proteins, intensifying Zn^{II}-displacement effects.^[10] Besides generating a pool of displaced metal ions, Cd^{II} interferes with its target's biophysical properties, namely stability, flexibility, and overall structure.^[11,12] Structure-interfering properties of Cd^{II} binding to Zn^{II}-containing proteins remain controversial because for decades Cd^{II} was used as a Zn^{II}-isostructural spectroscopic probe for Zn^{II}-binding proteins in UV spectrophotometric studies and ¹¹³Cd NMR spectroscopy.^[13–17] Although Cd^{II} and Zn^{II} ionic radii are relatively similar and displacement is usually one-to-one, in terms of stoichiometry and coordination sphere, their binding to a target protein could potentially generate a different structural outcome. The presented scientific problem of Zn^{II}-to-Cd^{II} substitution and its impact on zinc-binding proteins have been extensively studied; however, all published data are focused on intramolecular sites, mostly of zinc finger domains and metallothioneins. Effects of this substitution are not uniform and involve no, or very slight, changes in structure and function,

[a] M. Padjasek, O. Kerber, Prof. Dr. A. Krężel
Department of Chemical Biology
Faculty of Biotechnology
University of Wrocław
Joliot-Curie 14a, 50-383 Wrocław (Poland)
E-mail: artur.krezel@uwr.edu.pl

[b] Dr. M. Maciejczyk, M. Pyrka
Department of Physics and Biophysics
Faculty of Food Science
University of Warmia and Mazury in Olsztyn
Oczapowskiego 4, 10-719 Olsztyn (Poland)

[c] Dr. M. Nowakowski, Prof. Dr. W. Koźmiński
Faculty of Chemistry
Biological and Chemical Research Center
University of Warsaw
Żwirki i Wigury 101, 02-089 Warsaw (Poland)

Supporting information and the ORCID identification number(s) for the author(s) of this article can be found under:
<https://doi.org/10.1002/chem.201904942>.

© 2019 The Authors. Published by Wiley-VCH Verlag GmbH & Co. KGaA. This is an open access article under the terms of the Creative Commons Attribution License, which permits use, distribution and reproduction in any medium, provided the original work is properly cited.

like in the case of Sp1,^[18] Tramtrack,^[19] SUP37,^[20] or Ros87,^[21] as well as significant alterations of the domain fold, in the case of XPA,^[5,22,23] p53,^[24] or MTF-1.^[25]

Herein, we aim to illustrate for the first time how this phenomenon affects the intermolecular zinc-binding site by investigating Cd^{II} binding to the central fragment of *Pyrococcus furiosus* (*P. furiosus*) Rad50 protein. Rad50 is a constituent of the MR(N/X) (Nbs1/Xrs2 is distinctive for eukaryotes) complex responsible for double-stranded DNA damage signaling and repair. Active as a dimer, it consists of two protomers with a typical structure for the SMC protein family: a very long anti-parallel coiled-coil (cc) segment that connects two apexes of the protein (i.e., the globular DNA-binding ATPase domain), and the zinc hook domain responsible for dimerization by formation of a tetrathiolate Zn(CXXC)₂ coordination sphere (Figure 1).^[26,27] The overall dimeric assembly of the MR(N/X) complex is not well-defined, and data from electron and atomic force microscopy present multiple conformations of the complex ranging from open-circular-like to closed-rod-shape-like.^[26,28–30] Such alternating behavior seems to be a common feature of the SMC protein family and, for Rad50 in particular, could potentially allow mechanically driven functional diversification; for example, switching between pathways of

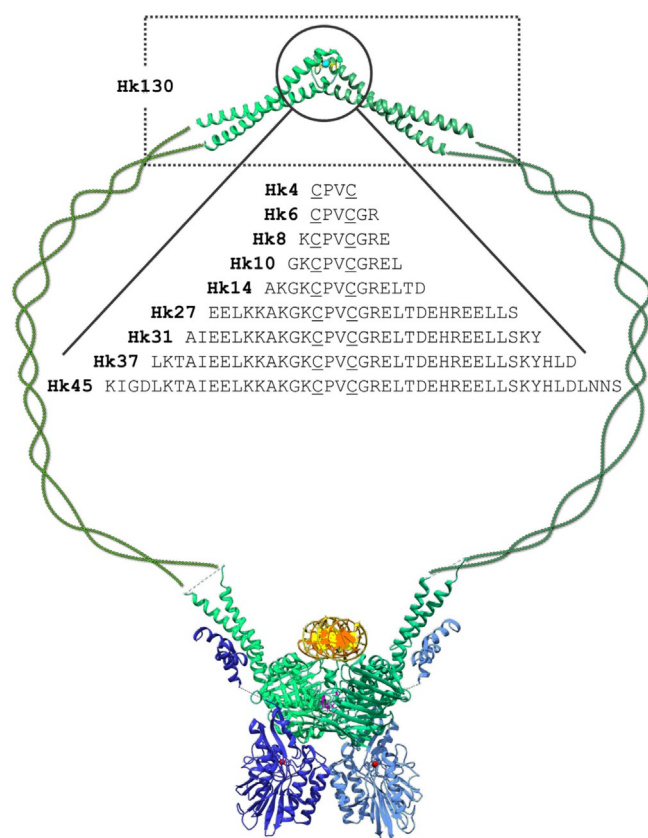


Figure 1. Architecture of the MR(N/X) complex with Rad50 fragments (Hk4–Hk130) investigated in this study. Green, blue, and yellow represent two Rad50, two MR, and one DNA molecule, respectively. Structural representation is based on the crystal structure of a central 112-amino-acid-long Rad50 (*P. furiosus*) fragment with Hg^{II} (PDB code: 1L8D) and the globular apex of a MR complex from *Methanocaldococcus jannaschii* bound to DNA (PDB code: 5DNY).

DNA damage repair. This process, however, could only be accommodated through specific flexibility of both globular and zinc hook apexes, the former of which has already been documented^[31] but the latter remains hypothetical. We hereby present an insight into molecular bases of Cd^{II} toxicity and indirect genotoxicity, taking into account the impact of Cd^{II} on Rad50's dimer stability and quaternary structure that could potentially result in abrogation of the major DNA damage response (DDR) pathway (and subsequent DNA lesions, chromosomal aberrations, and carcinogenesis).

Previous studies on the central fragment of the zinc hook domain of the Rad50 protein from *P. furiosus* demonstrated that this fold forms an extremely stable complex with Zn^{II}.^[32,33] The molecular basis of this high stability has been analyzed by using a set of hook model peptides (Hk) containing a -CPVC-binding motif with increased peptide flanks from both ends (Hk4–Hk45).^[32] The results indicated that the formation of a hook homodimer (Zn(Hk)₂) occurs in a stepwise manner starting from the formation of the ZnHk complex, followed by association of another Hk molecule. The increased difference in stability of the two complexes with rising peptide length favors the formation of the Zn(Hk)₂ species. The existence of an equimolar complex being in equilibrium with a dimer could be of high importance and suggests a possibility of readily exchangeable Rad50 molecules during cellular processes, which is believed to be the requirement for MRN native functions.^[34,35] Keeping in mind the toxic effect of Cd^{II} on zinc finger domains of transcription factors and other zinc-sulfur proteins associated with DNA processing, we aimed to examine the impact of Cd^{II} binding on the Rad50 protein using a well-described model from *P. furiosus*,^[32,33] which would be the first intermolecular zinc-binding site analyzed in terms of Cd^{II} attack. The aim of this study was threefold: 1) to demonstrate how strongly Cd^{II} ions bind to the Rad50 protein, 2) to show whether or not Cd^{II} ions are able to replace Zn^{II} in the cellular timescale, and finally, 3) to analyze how Cd^{II} binding affects the Rad50 hook structure in a way that could translate into functional alterations of Rad50 and the entire MRN complex.

Results and Discussion

In the first stage of the study, we examined whether Cd^{II} is capable of binding in the same stoichiometric model as Zn^{II} and whether it forms more stable complexes allowing Cd^{II} to exchange Zn^{II} from the hook domain. To assess if the structure and stability of Cd^{II} complexes rely on a similar structural basis to that of Zn^{II}, we used a series of zinc hook (Hk) peptides ranging in length from 4 to 130 amino acid residues (Hk4–Hk130) (Figure 1). Peptide Hk45 has been recognized as a fragment which, as a Zn^{II} complex, possesses all residues that form intermolecular contacts and contains both α -helical and β -hairpin regions of the domain.^[33] Peptides Hk4, Hk6, Hk10, and Hk14 were used to investigate metal-coupled formation of the β -hairpin. The remaining peptides (Hk27, Hk31, and Hk37) were applied for investigation of any important changes occurring in the vicinity of the region between the β -hairpin and the elongated domain (about 45 amino acid residues). The lon-

gest Rad50 protein fragment, containing 130 amino acid residues, was used as a Rad50 protein model containing a long coiled-coil fragment to examine whether effects occurring in minimal fragments are transferred to other protein regions and vice versa.

Spectroscopic analysis of Cd^{II} binding to the hook motif

Binding of Cd^{II} to hook peptides was monitored using several spectroscopic methods including spectrophotometry and spectropolarimetry for acetylated and amidated peptides, as well as fluorimetry and fluorescence anisotropy in the case of fluorescently labeled peptides. Far-UV circular dichroism (CD) titrations, performed by the addition of Cd^{II} to metal-free peptides at pH 7.4 in the presence of tris(2-carboxyethyl)phosphine hydrochloride (TCEP) (used as a non-metal-binding reducing agent),^[36] demonstrated extensive conformational changes for most investigated peptides upon Cd^{II} coordination (Figure 2a and Figure S1, Supporting Information). Spectrophotometric titration in the same region showed formation of a band with the maximum between 230 and 250 nm. This band corresponds to ligand-to-metal charge transfer (LMCT) events, and it is typical for CdS₄ metal centers found in tetrathiol-containing ligands, such as Zn(Cys)₄ (Figure S2, Supporting Informa-

tion).^[37–39] Both CD and UV/Vis spectra demonstrate a sharp inflection in the titration curves at a 1:2 Cd^{II}-to-peptide molar ratio, which confirms the formation of predominantly Cd^{II}-mediated homodimers: ML₂ complexes (Figure 2b). However, in the case of Hk27, Hk31, and Hk45, the formation of CdHk (ML) complexes also occurs. The largest difference in stability between ML and ML₂ complexes is observed for Hk27, which is reflected by two visible inflection points, whereas the Hk6, Hk10, and Hk14 peptides demonstrate the strongest tendency to form only dimeric species, similarly to the study of Zn^{II} complexes^[33] (Figure 2 and Figure S2, Supporting Information). In the case of Hk130, the CD spectra changes slightly (Figure 2a), which complicates stoichiometric analysis. However, spectrophotometric titration in the UV range clearly shows the formation of the Cd(Hk130)₂ homodimer, which is the predominant species (Figure 2b and Figure S3, Supporting Information). Depending on the examined peptide, the Cd(Hk)₂ complex adopts different conformations, as indicated by the distinct CD spectra. The structural changes obtained during Cd^{II} coordination can be compared qualitatively based on the differential spectra obtained through the spectral subtraction of free Hk peptide from their complexes with the metal ion (Figure 2c). Both types of spectra, together with their molar ellipticity, indicate the formation of a β-hairpin-like structure in the case of

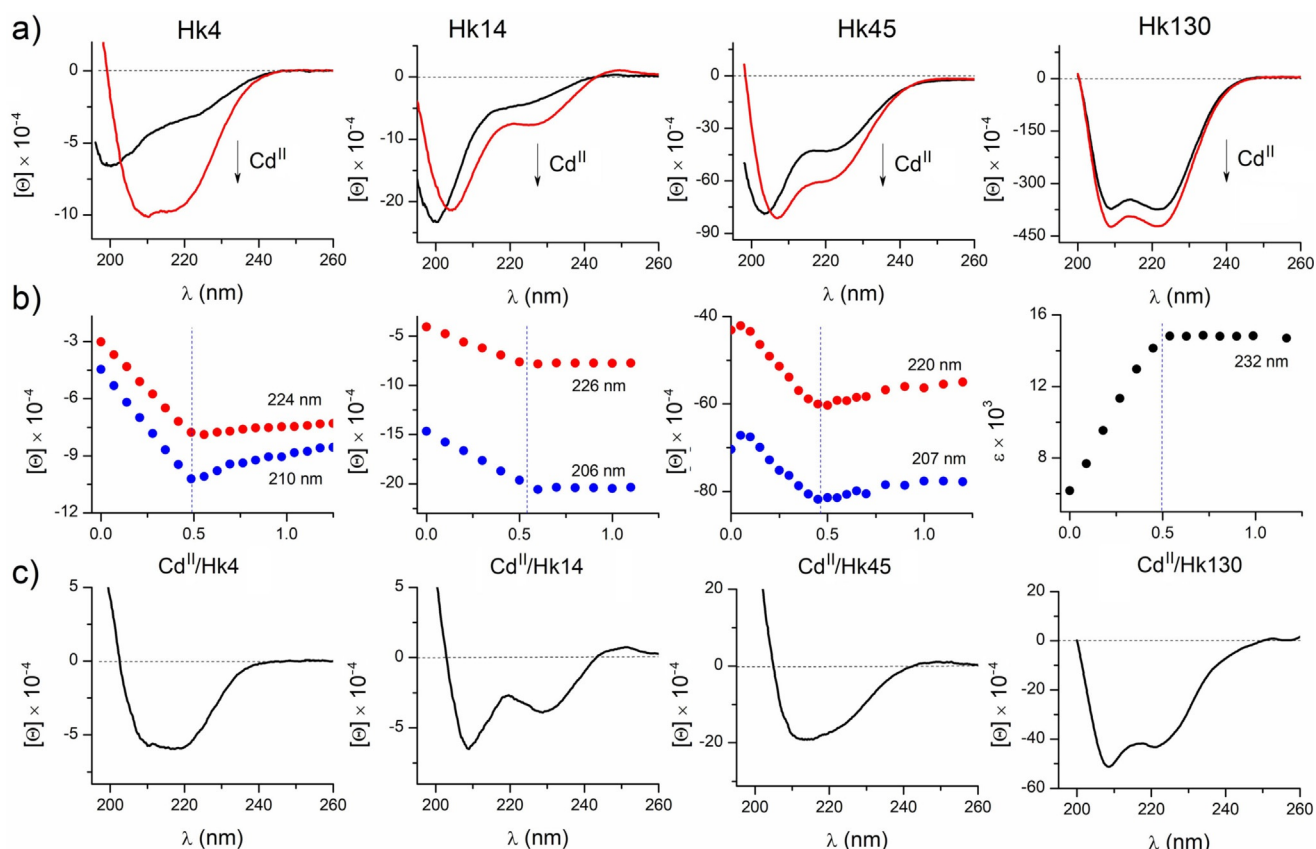


Figure 2. Cd^{II} binding to selected hook peptides recorded by CD and UV/Vis spectroscopy in 20 mM Tris-HCl buffer, pH 7.4, $I=0.1$ M. a) CD spectra of the apo form (black line) and the complex at a Cd^{II}-to-Hk peptide molar ratio of 0.5 (red line). b) Dependence of the ellipticity (Hk4, Hk14, Hk45) and absorbance (Hk130) at listed wavelengths on the Cd^{II}/Hk molar ratio. c) Differential CD spectra of hook peptides obtained by the subtraction of the spectra of free peptides from the spectra of Cd(Hk)₂ complexes. $[\Theta]$ and ϵ refer to molar ellipticity (in deg cm² dmol⁻¹) and molar absorption coefficient (in M⁻¹ cm⁻¹), respectively.

Cd(Hk14)₂ and mixed β -hairpin and helical structures in the case of Cd(Hk45)₂. The case of the longest Hk130 peptide is certainly different due to a long helical structure (more likely being a part of coiled-coil structure) that is already present in the metal-free form. The Cd^{II} binding to this protein fragment causes only small changes in the CD spectra, indicating additional structurization in the central metal binding part and parallel stabilization of the coiled-coil structure. Although the peptide backbone contribution is evident, one has to account for the Cd-S LMCT contribution in the overlapping region. Nonetheless, the backbone-related transitions presented herein are around 10–20 times stronger; hence, the Cd^{II}-binding contributions are significantly overshadowed and do not influence the qualitative assessment.^[37]

Metal-coupled β -hairpin formation in the middle of the zinc hook upon Cd^{II} complexation has been demonstrated by using a minimal N-terminally dansylated Hk14 peptide with a tryptophan residue placed at its C-terminus. Figure 3 (inset) shows the peptide's emission spectra when the tryptophan (Trp) residue is excited at 290 nm. Emission spectra demonstrate a fluorescence resonance energy transfer (FRET) effect between Trp and dansyl (Dns) residues, but the efficiency shows that both donor and acceptor are far away in the metal-free peptide, indicating the disorganized nature of the Hk14 peptide.^[32] When Cd^{II} is bound, and the homodimer is formed, the intensity of Trp significantly decreases while the intensity of the acceptor

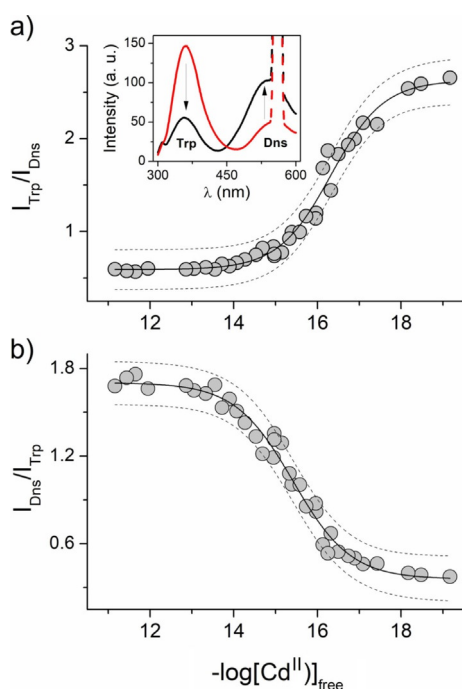


Figure 3. Cd^{II} binding to 5 μ M fluorescently modified Hk14 investigated fluorometrically under controlled free Cd^{II} conditions (HEDTA, EDTA, and TPEN competition) in 50 mM 4-(2-hydroxyethyl)piperazine-1-ethanesulfonic acid sodium salt (HEPES) buffer, pH 7.4, $I = 0.1$ M. a) Tryptophan-to-dansyl intensities ratio ($I_{\text{Trp}}/I_{\text{Dns}}$) changes. The inset demonstrates the emission spectra of free (black line) and Cd^{II}-bound (red line) Hk14. b) Dansyl-to-tryptophan intensities ratio ($I_{\text{Dns}}/I_{\text{Trp}}$) changes. Ratios were fitted to Equations (2) and (3), according to a protocol by Pomorski et al.^[52] Dashed lines represent a plot confidence of 95%.

increases, demonstrating a substantial efficiency increase.^[40,41] Taking into account the Förster radius of the Trp–Dns FRET pair, being between 21 and 24 Å, it is likely that this FRET efficiency change may be attributed to the proximity of both fluorophores around this range or rather below it.^[42] Indeed, the molecular dynamics simulation of Hk14 in the Cd^{II} complex (see Supporting Information for more details) shows that the estimated average distance between donor and acceptor in the Cd^{II} complex is (12.7 ± 2.5) Å. Similar FRET efficiency change upon metal binding has been observed for the Hk14 peptide and several of its mutants upon Zn^{II} complexation.^[32] However, the change occurring in the case of Cd^{II} is much more pronounced than that of its Zn^{II} counterpart, suggesting either more compact structure of a protomer or smaller distance between the N- and C-termini of a single protomer or between opposite termini of both protomers in Cd(Hk)₂. The hook structure, even in its minimal fold, is highly sensitive to any close-occurring changes. Our previous study showed that alanine scanning in the Hk14 sequence may affect the FRET effect significantly, indicating that even one non-metal-binding residue substitution may impact the hook's global structure.^[32] Moreover, changes occurring in the further region of the full domain also affect the structure and stability of formed complexes; this has been shown by using a longer peptide model as well as in vivo tests on the full MRX complex.^[43] Mutations of the hook domain's Cys-neighboring amino acids alter DNA damage repair and signaling functions of the entire complex, proving that alteration of the hook motif is transferred to the globular parts of the MRN complex, presumably through the coiled-coil region, and render it abrogated.^[44,45]

To thoroughly investigate the Cd^{II} ion's impact on the Rad50's zinc hook domain's assembly, we turned to anisotropy decay analysis. Measuring time-resolved anisotropy change provides vast analytical opportunities and gives insights into protein dynamics, dimensions, as well as protomer arrangement in oligomeric species. N-terminally FAM-labeled (FAM = 5(6)-carboxyfluorescein) *P. furiosus* Rad50 Hk14 and Hk45 were subjected to an anisotropy decay experiment either as apo forms, Zn^{II}/Cd^{II}-loaded, or analyzed after overnight incubation in a set of metal buffers. We focused our attention on one major parameter derived from anisotropy decay analysis: rotational correlation time [τ_r , Eq. (1)], which delivers information about molecular dimensions in terms of their diffusion capability in a solvent, for which I is intensity, r_{inf} is residual anisotropy, and τ_{r1} and τ_{r2} and B_1 and B_2 are rotational correlation time and amplitude, respectively, for both exponentials. Because the τ_r parameter describes how fast the fluorophores rotate, thus decreasing their anisotropy, it is directly correlated with the hydrodynamic radius of the emitting molecules.^[42]

$$I_r(i) = r_{\text{inf}} + B_1 \exp\left(\frac{-i}{\tau_{r1}}\right) + B_2 \exp\left(\frac{-i}{\tau_{r2}}\right) \quad (1)$$

The rotational correlation time parameter differs significantly for Zn^{II} and Cd^{II} complexes, which is clearly visible from plots of τ_r against a range of free metal ion concentrations (Figure 4). These results demonstrate that τ_r for both peptides

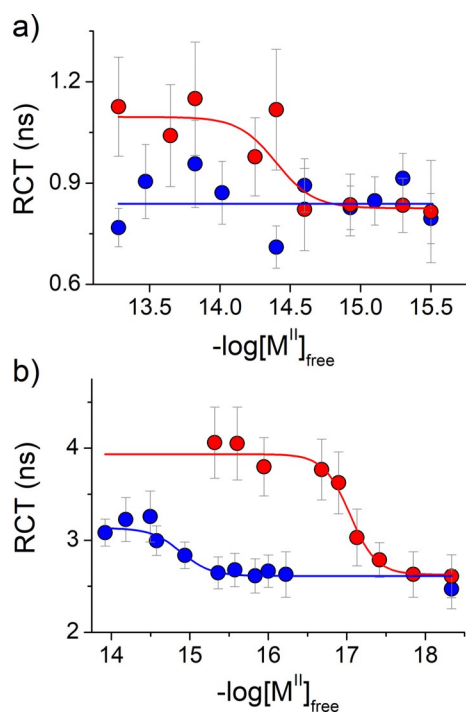


Figure 4. Rotational correlation time (RCT) changes of 500 nm FAM-labeled a) Hk14 and b) Hk45 presented as a function of the molar concentration of free Zn^{II} or Cd^{II} ($-\log[M^{II}]_{\text{free}}$) in HEPES buffer pH 7.4. Gray and red circles represent data from Zn(Hk)₂ and Cd(Hk)₂ experiments, respectively. Error bars represent standard deviation errors from two-exponential fitting of reconvolution anisotropy spectra (see the Supporting Information for more details).

increases with free metal ion concentration, as a result of metal-ion-induced dimerization, but the increase from metal-free to metal-bound form is around 30% higher for a Cd^{II}-binding event than that of Zn^{II}. The experiment suggests that Hk14 and Hk45 molecules in Zn^{II} and Cd^{II} complexes present different dimer arrangements with different hydrodynamic diameters, the former being smaller than the latter.^[42,46] Taking into account that the Cd^{II} ionic radius (109 pm) is slightly larger than the Zn^{II} radius (88 pm),^[10] this trait feels natural. However, it seems that swelling of the Rad50 dimer interface caused by incorporating a bigger metal ion is transferred further down through both protomers, changing the overall quaternary structure of the analyzed dimers.

Our approach possesses one major intrinsic obstacle that prevents precise volumetric measurement of analyzed dimers; as a result of the homo-labeling setup, homo-FRET events are very likely to occur between two FAM-labeled N-termini of Rad50 dimers, which results in an additional route of anisotropy decay. We speculate that homo-FRET transfer is represented as an additional decay time; however, it is too fast to allow quantitative assessment of differences between alternatively composed hook dimers. To resolve whether a homo-transfer's impact on anisotropy decay overshadows differences in molecular volume, we analyzed initial anisotropy values for both complexes. Initial anisotropy (not fundamental anisotropy, which is constant for 5(6)-carboxyfluorescein and equals 0.38) would be significantly affected by the homo-FRET phenom-

on, making it an ideal control parameter to ascertain the validity of this approach.^[42] Interestingly, initial anisotropy values for complexes with Zn^{II} were a little higher than those of complexes with Cd^{II}, suggesting homo-FRET of higher efficiency for the latter (Figure S4, Supporting Information). This means that differences in rotational correlation time are probably more pronounced, and the τ_r value for Cd(Hk)₂ may be in fact higher than what we have observed.

Determination of stability constants of Cd^{II} zinc hook complexes

As demonstrated in the spectroscopic studies, Cd^{II} titration curves of Hk peptides demonstrate isotherms of complex formation with a sharp inflection point, which clearly indicate that affinity of the studied hook peptides towards Cd^{II} is high, and direct spectroscopic stability constant determination would not be feasible without risk of their underestimation.^[47,48] Therefore, to determine actual stability constant values of the formed Cd^{II} complexes, several approaches were used. The first one and the most informative regarding the stoichiometric model and cumulative stability constants (formation constant β_{ijk} of the M_iH_jL_k complex, which includes the protonation state of the ligands coordinated to the metal ion) was potentiometry. However, as a result of the limited number of residues with acid-base properties, which is a requirement for this method, it was applied here only for Hk4–Hk14 peptides.^[49] The obtained results confirmed that ML and ML₂ stoichiometries of the complexes are formed during complexation and are variously protonated depending on the peptide chain length (Figure 5). Table 1 presents cumulative constants of all peptides investigated potentiometrically as well as the pK_a values of deprotonating groups. Species distribution presented in Figure 5 shows that the ML₂ (M = Cd^{II}) complex is formed at low pH (from about 4 and 3.5 for Hk4 and Hk14, respectively) and is stable up to basic pH. For comparison, Zn^{II} complexes of the same peptides are formed at around 0.5 unit higher in pH, indicating a significant difference between the two metal ions. This pH difference in dimeric complex formation is demonstrated by approximately two-orders-of-magnitude lower stability constants for Zn^{II} complexes when compared to Cd^{II} ones, although this difference varies depending on the peptides' length (Table 1).^[33]

Given that cumulative stability constants are pH-independent, the direct comparison of affinities between particular ligands or metal ions at certain pH is impossible without consideration of K_a values of metal-free ligands, which differ between each other. To present potentiometric data in a comparable way (with conditional constants determined spectroscopically), we calculated the formation constant K₁₂ of the Cd(Hk)₂ complexes valid for pH 7.4 as shown below [Eq. (2)]:

$$K_{12} = \frac{[\text{Cd}(\text{Hk})_2]}{[\text{Cd}^{II}][\text{Hk}]^2} \quad (2)$$

in which [Hk] is the sum of all metal-free Hk species with variously protonated states as well as fully deprotonated species

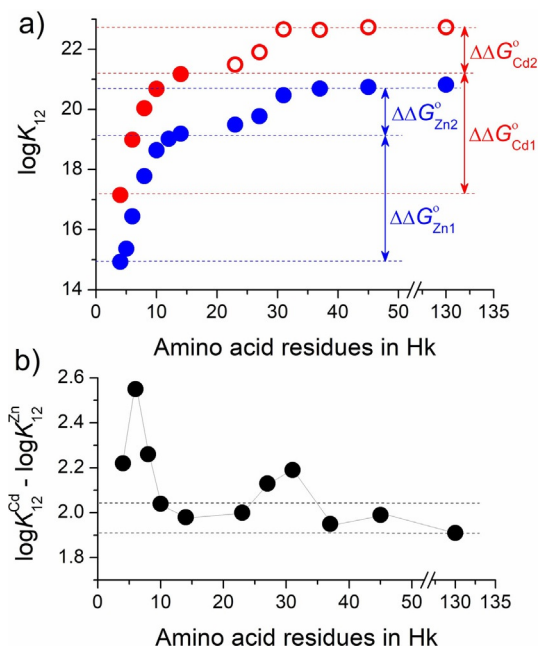


Figure 6. Comparison of conditional K_{12} constants ($\log K_{12}$) of $\text{Cd}(\text{Hk})_2$ and $\text{Zn}(\text{Hk})_2$ complexes at pH 7.4 varying in length of the zinc hook peptide. a) Blue circles correspond to Zn^{II} complexes determined previously.^[33] Red circles represent constants of Cd^{II} complexes determined herein potentiometrically (solid circles) and from competition with metal complexes (open circles). b) Differences in $\log K_{12}$ between Cd^{II} and Zn^{II} complexes. Dashed lines indicate the range of complex stability resulting only from metal-ion exchange.

Table 1. Cumulative protonation and Cd^{II} stability constants ($\log \beta_{ijk}$)^[a] of hook peptide complexes determined potentiometrically at 25 °C, $I = 0.1 \text{ M}$ (from KNO_3).^[b,c]

Species	Hook peptide ($\log \beta_{ijk}$)				
	Hk4	Hk6	Hk8	Hk10	Hk14
HL	9.372 ± 0.03	9.01 ± 0.04	10.65 ± 0.02	10.64 ± 0.04	10.80 ± 0.03
H ₂ L	17.52 ± 0.02	16.86 ± 0.02	19.75 ± 0.02	19.48 ± 0.03	20.48 ± 0.01
H ₃ L	-	-	27.57 ± 0.03	26.85 ± 0.02	39.19 ± 0.02
H ₄ L	-	-	31.81 ± 0.02	31.02 ± 0.04	36.48 ± 0.02
H ₅ L	-	-	-	-	40.89 ± 0.03
H ₆ L	-	-	-	-	44.88 ± 0.04
CdH ₂ L	-	-	-	-	33.33 ± 0.04
CdHL	-	-	23.19 ± 0.04	22.96 ± 0.04	-
CdL	12.58 ± 0.04	12.33 ± 0.03	-	-	-
CdH ₄ L ₂	-	-	-	-	65.26 ± 0.07
CdH ₃ L ₂	-	-	-	-	56.10 ± 0.09
CdH ₂ L ₂	-	-	45.86 ± 0.02	45.20 ± 0.05	46.80 ± 0.04
CdHL ₂	-	-	36.61 ± 0.03	37.66 ± 0.06	36.55 ± 0.03
CdL ₂	22.74 ± 0.03	23.38 ± 0.02	n.d.	n.d.	n.d.

[a] $\beta(\text{M}_i\text{H}_j\text{L}_k) = [\text{M}_i\text{H}_j\text{L}_k] / ([\text{M}]^i [\text{H}]^j [\text{L}]^k)$, in which [L] is the concentration of the fully deprotonated zinc hook peptide. [b] Standard deviations are given as provided by SUPERQUAD calculations. [c] n.d. denotes 'not determined' under used conditions.

at pH 7.4 being in equilibrium in the $\text{Cd}(\text{Hk})_2$ complex. Such conditional constants demonstrate that affinity of Hk peptides towards Cd^{II} increases together with the peptide length from about 10^{17} M^{-2} for Hk4 to about 10^{21} M^{-2} for Hk14 (Table 2). However, the largest increase in stability is observed between Hk6 and Hk10, similarly to Zn^{II} complexes (Figure 6), suggest-

Table 2. Conditional formation constants (K_{12}) of $\text{Cd}(\text{Hk})_2$ complexes and corresponding competitiveness indexes (CI) obtained from potentiometric, CD, and fluorometric (FL) data. Standard error is provided only for data obtained in competition and exchange experiments. Potentiometry-derived K_{12} values were calculated from data presented in Table 1.

Hook peptide	Method of determination	$\log K_{12}$	CI ^[a]
Hk4	potentiometry	17.15	13.85
Hk6	potentiometry	18.99	15.69
Hk8	potentiometry	20.04	16.74
Hk10	potentiometry	20.68	17.38
Hk14	potentiometry	21.16	17.86
	FL competition	21.17 ± 0.05	17.87
Hk27	CD competition	21.96 ± 0.07	18.66
Hk31	CD competition	22.60 ± 0.09	19.30
Hk37	CD competition	22.64 ± 0.03	19.34
Hk45	CD competition	22.64 ± 0.05	19.34
Hk130	FL competition	22.73 ± 0.05	19.43

[a] CI is the logarithm of the apparent dissociation constant of the CdL complex (Cd^{II} complex of theoretical molecule Z), such as $[\text{CdZ}] = \sum_{ijk} [\text{Cd}_i\text{H}_j\text{L}_k]$ at given overall component concentrations. The concentrations of Z were set at 1 mM and those of Cd^{II} at 0.25 mM.

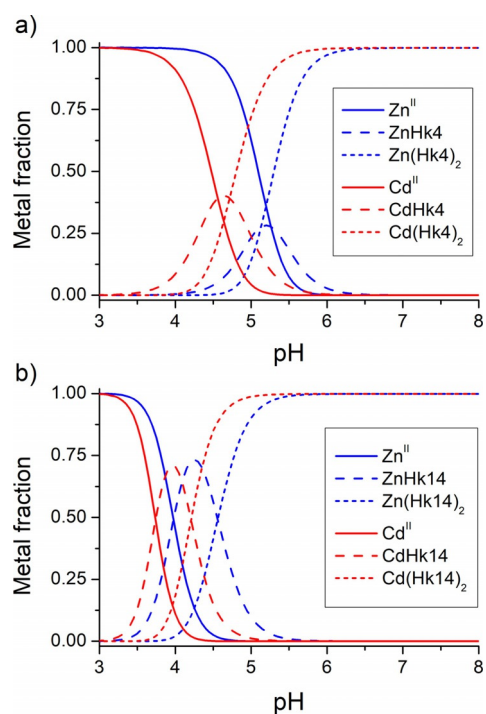


Figure 5. Molar species distribution of Cd^{II} and Zn^{II} complexes with a) Hk4 and b) Hk14 peptides calculated based on protonation and stability constants determined potentiometrically. Hk peptides and metal ion concentrations were set as 400 and 200 μM , respectively, as in the potentiometry experiments.^[32]

ing that Cd^{II} -mediated folding of the β -hairpin is the energy force that elevates stability of the hook domain, analogously to Zn^{II} complexes.^[32,33]

Although potentiometry is a good method for determination of stability constants of highly stable complexes, its application is limited to the number of acid-base groups, and it is difficult or impossible to use for proteins and their larger frag-

ments. Therefore, to determine K_{12} of Cd^{II} complexes with Hk27, Hk31, Hk37, Hk45, and Hk130 peptides, we applied CD-monitored competition with common metal complexes with well-established stability constants, such as HEDTA, EDTA, and TPEN.^[48,50] Because ellipticity changes of the Hk130 peptide are the smallest, CD data were supported by natural tyrosine fluorescence change, the intensity of which decreases upon Cd^{II} binding (Figure S5, Supporting Information). Figure 7 shows normalized ellipticity or fluorescence intensity as a function of free Cd^{II} ions, calculated using Hyperquad software based on protonation and stability constants of Cd^{II} -complexone com-

plexes.^[51] To determine K_{12} values, experimental data were first fitted to Hill's equation^[32] to obtain half-saturation points ($-\log[\text{Cd}^{\text{II}}]_{\text{free}}^{0.5}$). In the next step, K_{12} values were calculated according to Equation (2), assuming that the half-saturation point corresponds to the half of maximal concentration of $\text{Cd}(\text{Hk})_2$.^[32,33] Obtained K_{12} values with standard deviation error are presented in Table 2 and also illustrated in Figure 6 (open red circles), in which they overlap very well with K_{12} values obtained from potentiometry for shorter peptides (solid red circles). These results indicate acceptable data coverage between the two methods (potentiometry and spectroscopy).

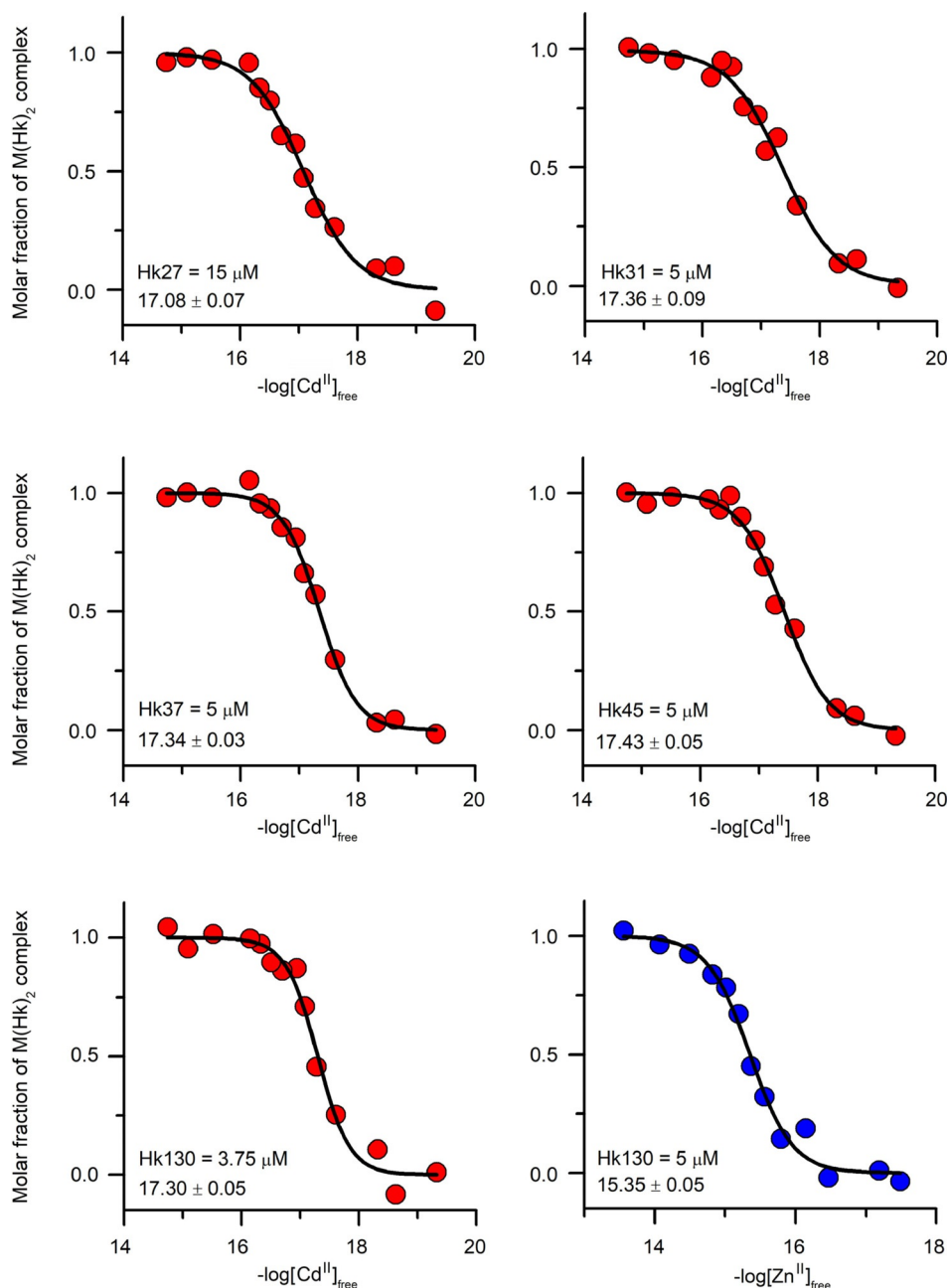


Figure 7. Isotherms of Cd^{II} (red circles) and Zn^{II} (blue circles) binding to Hk27, Hk31, Hk37, Hk45, and Hk130 in the presence of 25 μM metal chelators determined spectropolarimetrically or fluorometrically in 20 mM Tris-HCl buffer, pH 7.4, $I=0.1$ M. Peptides were used at various and listed concentrations. Data were fitted to the Hill equation, and the presented values correspond to half-saturation points ($-\log[\text{Cd}^{\text{II}}]_{\text{free}}^{0.5}$ and $-\log[\text{Zn}^{\text{II}}]_{\text{free}}^{0.5}$) used for K_{12} calculation (Table 2).

Because Hk14 was shown to be the minimal fold of extreme stability,^[32] its complex with Cd^{II} was herein investigated primarily and resulted in an additional set of competition data gathered for the fluorescently labeled Hk14 with Dns and Trp moieties. This type of modification enables assessment of wide dynamic range changes that guarantee the highest-quality data determination. Moreover, the presence of two bands corresponding to the donor and acceptor of the FRET pair makes this peptide a sensitive ratiometric sensor of free Cd^{II} concentration and conformational changes. Figures 3a,b demonstrate Trp/Dns (R_{Trp}) and Dns/Trp (R_{Dns}) ratios of intensity changes, respectively, as a function of free Cd^{II}. To determine the actual $-\log[\text{Cd}^{\text{II}}]_{\text{free}}^{0.5}$ value from the ratiometric study, we applied our normalizing equations that are based on fixed maximal and minimal intensities of Trp and Dns bands, independently, as described elsewhere.^[52] Application of these formulae to fluorescence intensity ratios resulted in actual $-\log[\text{Cd}^{\text{II}}]_{\text{free}}^{0.5}$ values of 15.8 and 15.7 for R_{Trp} and R_{Dns} , respectively, allowing further $\log K_{12}$ calculation to give 21.17. Formation constants obtained with this method are convergent with the values calculated from potentiometric data (Table 2).

Stability comparison of Cd^{II}-substituted hook domain with other Cd^{II} complexes

Our previous results have shown that the zinc hook domain is among the most stable Zn^{II} complexes found in proteins and their natural domains. For example, the Zn(Hk45)₂ complex is more stable than the most stable natural zinc fingers described so far, such as Sp1-3, MTF-1, or Zif268-2, when competing in the micromolar range with Hk45.^[33,47,53] When concentrations of both protein fragments decrease, zinc fingers demonstrate a higher tendency to bind Zn^{II}. Such behavior comes from the fact that the hook domain forms an ML₂-type complex, whereas zinc fingers and most other proteins form an ML-type complex. Our recent results obtained on various zinc domains with different Zn^{II}-to-protein stoichiometry, yet similar affinity, showed concentration dependence for metal-mediated complexes.^[54] Such concentration-dependent metal association might be an important feature for transient saturation and transient protein function. In light of these results, there are important questions of how Cd^{II} ions may affect zinc hook structure and function, and how Cd^{II} binding may affect possible transient saturation of the hook domain. To get closer to answering these questions and to properly order the cadmium hook in the stability hierarchy of Cd^{II} complexes with proteins, it is worth analyzing the literature in terms of stability data of Cd^{II} complexes of other proteins or peptide models. Table 2 presents the apparent formation constants of Cd(Hk)₂ at pH 7.4, calculated either from potentiometric data or determined by competition with complexones. Because of the fact that the hook motif forms an ML₂-type complex, direct comparison of its formation constant (K_{12}) with constants of complexes with ML stoichiometry of other ligands is impossible. To avoid this problem, we converted all formation constants present in Table 2 to the competitiveness index (CI), which has been shown previously to be useful for the comparison of affinities

of metal complexes with various stoichiometries.^[55,56] In principle, it simplifies any stoichiometry to M_xL_y, under certain reactant concentrations and is valid only when comparable ligands and metal ion are present in the same concentrations.^[56] Thus, a quick comparison of CI values of Cd^{II} hook complexes and other Cd^{II} complexes found in the literature (Table 3) shows that the investigated complexes, Hk14–Hk130, are the most stable found to date. The CI values of these Cd^{II} hook complexes are two-to-four orders of magnitude more stable (CI = 17–19) than the strongest ones with XPA zf (CI = 12.8),^[23] CadC (CI = 12.6),^[57] CmtR (CI = 12.2),^[58] or MT2 (CI = 14.4 for β -domain and 15.8 for α -domain).^[59] Moreover, the complexes investigated here are much more stable than the Cd^{II} complex with EDTA (CI = 13.6),^[60] consensus CP1 zf (CCCC) zinc finger (CI = 13.4),^[61] or short poly-Cys peptides known to form highly stable complexes with Cd^{II}, for instance Ac-YCSCSY or Ac-CC-NH₂, for which CI is 14.8 and 12.6, respectively.^[62,63] This brief overview clearly demonstrates that the zinc hook domain with substituted Cd^{II} must exhibit unique stabilization effects that elevate thermodynamic stability. Molecular reasons for such stability are discussed below.

Zn^{II}-to-Cd^{II} swap in zinc hook domain

Data presented above show that Cd^{II} complexes of the minimal and elongated hook domain are significantly more stable than Zn^{II} counterparts and other protein, peptide, and low-molecular-weight organic complexes. This should be reflected by an efficient Zn^{II} swap when Cd^{II} ions are added to the zinc hook domain. To examine experimentally how fast and efficient the substitution of metal ions occurs, we titrated the Zn^{II} complex of Hk14 and Hk45 with Cd^{II} and observed changes occurring in UV/Vis and CD spectra. This was possible due to the formation of energetically lower LMCT bands at 230–250 nm for Cd^{II} in comparison with those of Zn^{II} complexes.^[37–39] This effect has also been observed in CD spectra by bathochromic shift of ellipticity negative maxima and their intensity increase when Cd^{II} swap occurred. To measure the equilibrated states of the reaction during titration properly, the kinetics of Zn^{II}-to-Cd^{II} swap was examined first. Figure S6 (Supporting Information) indicates that in the case of both Zn(Hk14)₂ and Zn(Hk45)₂ complexes the time necessary for metal-ion-exchange completion is lower than 2 minutes, indicating rapid kinetics of the metal swap. Exchange for Hk14 was shown to occur under first-order kinetics with a rate constant calculated to be about 0.015 s⁻¹, and the rate for Hk45 is even faster and was impossible to determine under standard settings. When the Zn(Hk14)₂ complex was titrated with Cd^{II}, the metal exchange observed by an increase in the LMCT band intensity (Figure 8a) reveals almost direct exchange, indicating that the reaction is not only rapid but also highly efficient, as expected, due to the difference in stability constants of Cd^{II} and Zn^{II} complexes. Fivefold molar excess of Zn^{II} over Hk14 slows down the exchange in such a way that a higher concentration of Cd^{II} is necessary to swap the hook-bound Zn^{II}. This enables calculation of the formation constant K_{12} based on the fixed constant of Zn(Hk14)₂ and total Cd^{II} concentration (Figure 8b).^[54] The K_{12} values calcu-

Table 3. Affinities of selected low-molecular-weight ligands, peptides, and proteins for Cd^{II} collected across the literature that form highly stable complexes. Stability constants were determined under various conditions, which are listed. If not specified, values refer to pH 7.4. RT, pHT, CC, and n.c. refer to reverse titration, pH titration, competition with metal chelator, and not calculated, respectively. CI values derived from formation constants presented as 'not calculated' (n.c.) were determined from published log β_{ML} data from potentiometric analyses.^[38,39,62,63,83]

Ligand ^[a]	Reference	Method of determination	Conditions	Stoichiometry of the complex	Formation constant (log K)	CI
EDTA	[60]	potentiometry	100 mM KNO ₃	ML	13.6	13.6
HEDTA	[60]	potentiometry	100 mM KNO ₃	ML	13.1	13.1
TPEN	[60]	potentiometry	100 mM KNO ₃	ML	16.4	16.4
DTBA	[39]	potentiometry	100 mM KNO ₃	ML, ML ₂ , M ₂ L ₃	n.c.	12.8
DTT	[38]	potentiometry	100 mM KNO ₃	ML, ML ₂	n.c.	10.4
Ac-CC-NH ₂	[63]	potentiometry	100 mM KCl	ML ₂	n.c.	12.6
Ac-YCSCCY	[62]	potentiometry	100 mM NaClO ₄	ML, ML ₂	n.c.	14.8
Ac-EEGCCHGHE-NH ₂	[63]	potentiometry	100 mM KCl	ML, ML ₂	n.c.	12.5
γECγEC (PC2)	[83]	potentiometry	100 mM KNO ₃	ML, ML ₂	n.c.	10.7
XPA zf	[23]	UV/Vis RT	50 mM phosphate, pH 7.4	ML	12.8	12.8
CP1 zf (CCCC)	[61]	UV/Vis RT	100 mM HEPES, 50 mM NaCl, pH 7.0	ML	13.4	13.4
CP1 zf (CCCH)	[61]	UV/Vis RT	100 mM HEPES, 50 mM NaCl, pH 7.0	ML	11.2	11.2
CP1 zf (CCHH)	[61]	UV/Vis RT	100 mM HEPES, 50 mM NaCl, pH 7.0	ML	8.7	8.7
TT-2D zf	[84]	UV/Vis pHT	200 mM HEPES, 100 mM NaCl, pH 7.5	ML	8.5	8.5
MT2	[59]	UV/Vis pHT	5 mM Tris-HCl, 50 mM NaCl, pH 7.0	M ₇ L	14.4	14.4
					15.8	15.8
CmtR	[58]	CC	10 mM Bis-Tris, 400 mM NaCl, pH 7.0	ML	12.2	12.2
CadC	[57]	CC	5 mM MES, 200 mM NaCl, pH 7.0	ML	12.6	12.6

[a] DTBA = dithiobutanoic acid, DTT = DL-dithiothreitol, EDTA = ethylenediaminetetraacetic acid, HEDTA = N-(2-hydroxyethyl)ethylenediamine-N,N',N'-triacetic acid, TPEN = N,N,N',N'-tetrakis(2-pyridylmethyl)ethylenediamine, Bis-Tris = 2,2-bis(hydroxymethyl)-2,2',2''-nitrilotriethanol, MES = 2-(N-morpholino)ethanesulfonic acid.

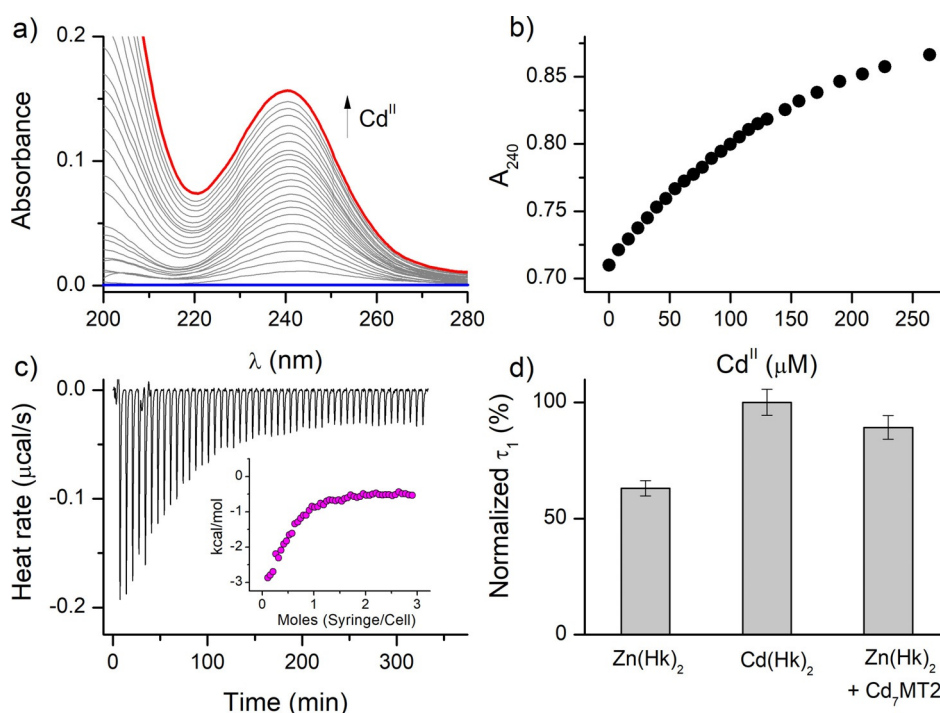


Figure 8. Zn^{II}-to-Cd^{II} swap in hook peptides illustrated by UV spectroscopy, ITC, and anisotropy decay analysis. a) Differential UV/Vis spectra of 100 μM Hk14 and 500 μM Zn^{II} titrated with Cd^{II}. b) Absorbance changes at 240 nm from a) illustrated as a function of increasing Cd^{II} concentration indicating metal-ion exchange. c) ITC analysis of 100 μM Hk14 with 250 μM Zn^{II} stepwise titrated with 1000 μM Cd^{II}, represented as a baseline-subtracted heat rate as a function of time. The inset shows heat per mole of titrant as a function of the Cd^{II}/Zn(Hk14)₂ molar ratio. d) Anisotropy decay analysis of 500 nm FAM-Hk45 presented as rotational correlation time changes normalized to the apo form (0) and Cd(Hk45)₂ of Zn(Hk)₂, Cd(Hk)₂, and Zn(Hk)₂ with equimolar Cd₇MT2. Error bars represent standard deviations from averaging four consecutive samples.

lated based on the exchange mode are slightly higher than the values obtained potentiometrically or in competition with

complexones (Table 2), probably due to intrinsically low resolution of the method in terms of stability determination^[47,53] and

were not included in further discussion. Nonetheless, the results prove that Zn^{II}-to-Cd^{II} swap is a fast and efficient process that can occur inside a cell, causing Cd^{II}-induced toxic effects.

To illustrate the Zn^{II}-to-Cd^{II} exchange event located inside Rad50's hook domain, we performed isothermal titration calorimetry (ITC) analysis in a manner similar to the previous approach. 100 μM Hk14 with 2.5-fold molar excess of Zn^{II} was titrated stepwise with 500 μM Cd^{II}. As shown in Figure 8c, Cd^{II} readily displaces the hook-bound Zn^{II} ion, which is represented as a slowly decreasing exothermic process (inset) of a tendency much like the one from the UV spectroscopy experiment (Figure 8b). Thermodynamics associated with the metal exchange reaction is discussed separately below.

Living organisms possess multiple factors that guard cells from Cd^{II} toxicity, with the two most important examples being glutathione (GSH) and metallothioneins. Regardless of the fact that GSH is present in the cytoplasm in millimolar levels, Cd^{II} maintains the capacity to infiltrate protein targets. It is a known fact that Cd^{II} accumulation in mammals occurs in soft organs, especially in the liver and kidneys.^[64–66] Metallothionein, found originally as a Cd^{II}-binding protein in the horse kidney cortex, binds this metal ion very tightly in two distinct clusters: four Cd^{II} ions in the α-cluster and three Cd^{II} ions in the β-cluster. However, isolated hepatic metallothionein from cadmium-toxicated mammals demonstrates a heterogeneous nature.^[67] Metallothionein binds at the same time Cd^{II} as well as Zn^{II} ions at various molar ratios; however, only a Cd₅Zn₂MT species was characterized structurally, and the crystal structure of this species is the only X-ray structure of mammalian MTs.^[68,69] In this study, by using Cd^{II}-reconstituted metallothionein-2, we aimed to examine whether tightly bound Cd^{II} ions by this protein can be transferred to the zinc hook domain of the Rad50 protein, which as a consequence could shed a light on Cd^{II} ion distribution in cells.

It is worth mentioning that seven Cd^{II} ions are bound in MT2 with two distinct affinities: three ions corresponding to the β-cluster with averaged log *K* = 14.4 and four bound in the α-cluster with log *K* = 15.8, which is in contrast to that of zinc MT2.^[58,70,71] Stability data obtained in this study suggest that Cd^{II} could be easily transferred from human Cd₇MT2 to the hook domain. To examine Cd^{II} transfer from MT2, which demonstrates strong absorption in the UV range due to LMCT bands occurring between the Cys residue and Cd^{II}, we used the fluorescently labeled Hk45 peptide and monitored anisotropy changes associated with this process. Our study showed that anisotropy decay of Zn^{II} and Cd^{II} hook complexes differs in terms of rotational correlation time values, which enables its use for type-detection of metal ions bound to peptides.

In the first step of metal swap, similarly to free Cd^{II} ion substitution, we examined the kinetics of the transfer. Fluorescein emission changes presented in Figure S7 (Supporting Information) indicate that the kinetics is very fast and that the reaction occurs completely in the time window below 1 minute. Kinetics of the swap seem to be equally fast for Cd^{II} alone (i.e., not bound to MT2) and fully Cd^{II}-metalated MT2. To show that both act in a similar fashion, we examined Zn(Hk45)₂ and Cd(Hk45)₂ with either addition of Cd^{II} or Cd₇MT2a. The control

sample's rotational correlation time, being in this particular case of Cd(Hk45)₂, was similar after separate addition of Cd^{II} and Cd₇MT2a in 0.5 and one molar equivalents, respectively (Figure S8, Supporting Information). However, for the Zn(Hk)₂ sample the parameter changed towards Cd^{II}-specific values, both for Cd^{II} and Cd₇MT2a additions (Figure 8d). Overall, the results show that Zn^{II}-to-Cd^{II} swap occurs even with the additional Cd^{II}-chelating component, and we suggest that it may be a relevant cellular process where MT is one of the major barriers against Cd^{II} toxicity.

Structure determination of Zn^{II}- and Cd^{II}-substituted hook domain

All spectroscopic and thermodynamic studies obtained in this report demonstrate that the minimal fragment of the hook domain (Hk14) forms a well-defined and highly stable structure as a complex with Cd^{II} ions. Stability constants obtained for longer models show that sequence elongation does not affect the stability of the complex significantly, suggesting that folding of the hook domain starts from the short 14-amino-acid-long fragment responsible for Rad50 dimerization. Although a *P. furiosus* Rad50 zinc hook domain's crystal structure was solved more than two decades ago, we are still missing a structure of a Zn^{II}-loaded complex because the solved one was actually a mercury hook (Hg(Hk112)₂, PDB code: 1L8D).^[26] In light of the results presented above, we speculate that the zinc hook may be in fact structurally different in solution, given that the Cd^{II}-loaded hook seems to possess a different dimeric arrangement. Thus, we aimed to determine structures of this motif to provide a new look at this alluring interprotein site. For this reason, we obtained 5 mM Zn^{II} and Cd^{II} complexes of the Hk14 hook model and performed a number of one- and two-dimensional NMR spectroscopic experiments, including ¹H–¹³C HSQC, TOCSY, and NOESY, obtaining 130 and 190 NOE peaks for Zn^{II} and Cd^{II}, respectively. From these, 20 and 15 peaks for Zn^{II} and Cd^{II} complexes, respectively, were rejected at the initial assignment.

The ten lowest-energy structures of Zn(Hk14)₂ and Cd(Hk14)₂ obtained with PROT and CRYST procedures (with hydrogen-bond restraints obtained from protection factors and crystal structures, respectively, as explained in the Supporting Information) are shown in Figure 9. The statistics of violated restraints are collected in Table S5. The energy of violated restraints is relatively low for both Zn(Hk14)₂ and the first conformation of Cd(Hk14)₂. For the second conformation of Cd(Hk14)₂ computed with CRYST restraints, significant (> 0.5 Å) violations of two hydrogen bonds (Val7 N–Cys5 S and Arg10 N–Cys8 S) were observed in 3 out of 10 structures, leading to a substantial rise in the average energy of restraints. Therefore, we ran additional calculations without restraints put on these two weak hydrogen bonds and obtained structures with reasonable mean energy of NOE and hydrogen-bond restraints (see Table S5). Calculations with PROT restraints led to structures with very small violations of H-bond restraints, but violations of NOE restraints increased in comparison to the structures obtained with CRYST restraints; although only 2 out of

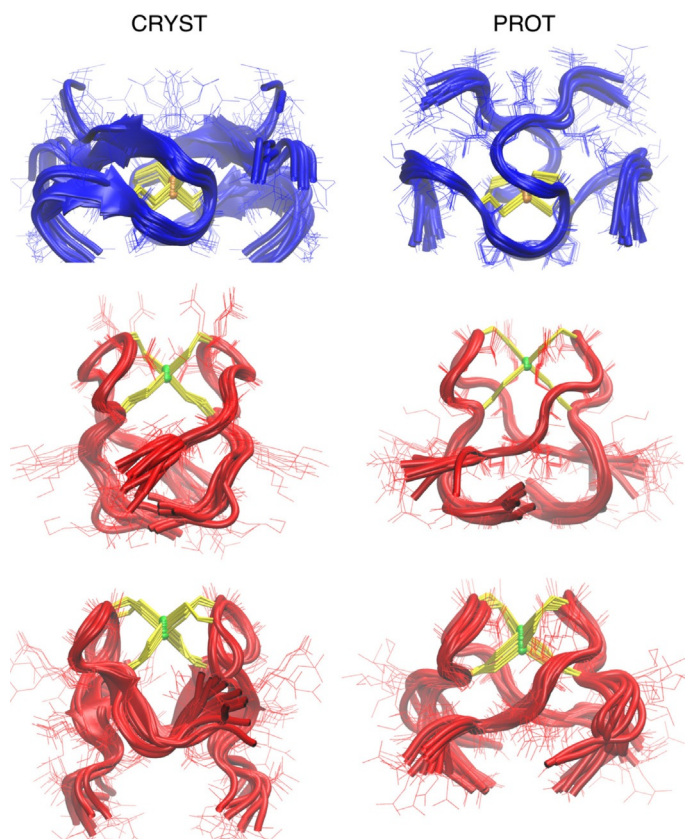


Figure 9. Ensembles of ten dimeric structures of the Hk14 peptide with Zn^{II} (blue chains) and Cd^{II} (red chains). Structures in the left column were determined with the CRYST procedure, and structures in the right column were determined with the PROT procedure (see the Supporting Information). Cysteine side chains are shown in yellow stick representation, and Zn^{II} and Cd^{II} are shown as orange and green spheres, respectively. The relative arrangement of loops of two analogous complexes with different ions differs significantly (see Results and Discussion). Two structures of complexes with Cd^{II} (middle and lower rows) correspond to two sets of chemical shifts obtained from the NMR spectroscopic experiments. In the computation procedure for the bottom left structure, two weak N–S hydrogen-bond restraints were removed.

10 computed structures have severely violated NOE restraints (NOE energy close to 200 kcal mol⁻¹). Nevertheless, structures obtained for the second set of chemical shifts are similar to those obtained for the first set, as can be seen in Figure 9.

The structures of peptides with Cd^{II} and Zn^{II} have clearly different arrangements of chain termini (Figure 9 and Figure S9, Supporting Information). The N- and C-termini of both Hk protomers bound to Cd^{II} are located close to each other (red structures in middle and lower panels of Figure 9), whereas the termini of the same peptides bound to Zn^{II} are located on the opposite sides of the complex (blue structures in upper panel of Figure 9 and Figure S9, Supporting Information). Described structural differences may also be present in complexes of the investigated ions with longer Hk peptides, leading to different arrangements of helices forming coiled coils and a global structural change of the entire MR(N/X) complex. Nonetheless, further structural studies on longer protein fragments need to be undertaken to confirm this hypothesis.

Molecular bases of elevated stability

Data reported herein clearly show that the Rad50 hook complex with Cd^{II} is significantly more stable, by around two orders of magnitude in terms of K_{12} , compared with its physiological counterpart that is Zn^{II}. Moreover, having established the Cd^{II}-binding affinity of the central fragment of *P. furiosus* Rad50, we thereby documented the most stable Cd^{II}-peptide complex analyzed so far (Table 3). Such extreme stability is likely to be generated by multiple molecular factors, including enthalpic and entropic contributions from Cd–S bond formation and metal-induced nucleation, to name a few. Figure 6a and Table S6 (Supporting Information) show that formation constant K_{12} values of Cd(Hk)₂ complexes are almost proportionally shifted towards higher stabilities than those of Zn^{II} hook model complexes. This indicates that these two types of complexes behave similarly when the hook motif is elongated from both ends. In Figure 6a, blue and red arrows indicate two events of Gibbs free energy contribution for Zn^{II} and Cd^{II} complexation, respectively, demonstrated as an energy difference ($\Delta\Delta G_{Cd/Zn}^\circ$) as a function of peptide length. The first event occurs between 4 and 14 amino acid residues in the hook motif, and the second event (less pronounced) occurs between 23 and 45, which correspond to the metal-binding-induced formation of the β -hairpin and nucleation of the coiled-coil region, respectively.^[33] The difference between formation constants ($\log K_{Cd}^{12} - \log K_{Zn}^{12}$) is similar for Hk10, Hk14, Hk37, Hk45, and Hk130 and is 1.98 ± 0.04 , which corresponds to -2.7 kcal mol⁻¹ of Gibbs free energy and, with a high level of confidence, is correlated with increased contribution of bond formation enthalpy for Cd–S compared with that for Zn–S (Table S6, Supporting Information). However, the $\log K_{12}$ differences presented in Figure 6b demonstrate the presence of two regions where Cd^{II} complexes are even more stabilized than the rest of the length-differentiated peptide series. The first extra-elevated region occurs for hook peptides between Hk4 and Hk8 with a maximum at Hk6. This significant stability increase is very likely connected to differences in the ionic radii of both ions and the possibility of generating alternate torsion angles of peptide bonds or even diverse intra- and intermolecular connections.^[33] Another, less pronounced, region indicating an additional difference between the two metal-ion complexes is present at the amino-acid length of 31. This region is more complicated to explain, but we suggest it may be caused by a shift in the coiled-coil nucleation event towards shorter hook lengths for Cd(Hk)₂, which is somewhat supported by the CD data showing higher capacity for the hook's helical nucleation of Cd^{II} compared with that of Zn^{II}, judged by qualitative evaluation (Figure S10, Supporting Information).

To assess what thermodynamic processes are involved and how they affect the stability of Cd(Hk)₂, we performed ITC anal-

ysis of apo Hk4–45 titrated with Cd^{II} and Zn^{II} (Figures S11, S12, Supporting Information) to illustrate differences between complexation of both metal ions as well as the Zn^{II} complex titrated with Cd^{II} to visualize the energetic outcome of the Zn^{II}-to-Cd^{II} swapping phenomenon (Figure 8c). Figure 8c shows that Cd^{II} efficiently replaces Zn^{II} inside the hook motif, even in excessive Zn^{II} conditions. Moreover, it proves the existence of a favorable enthalpic contribution of the swapping event, which seems to be approximately $-2.6 \text{ kcal mol}^{-1}$, a value that corresponds well with the $-2.7 \text{ kcal mol}^{-1}$ value obtained from potentiometric and spectroscopic studies (Figure 6b and Table S6, Supporting Information). On the other hand, independent experiments with Zn^{II} and Cd^{II} titrations of apo peptides suggest that complex formation enthalpies of Zn(Hk14)₂ and Cd(Hk14)₂ are -18.1 and $-21.6 \text{ kcal mol}^{-1}$, respectively, which gives $-3.5 \text{ kcal mol}^{-1}$ for $\Delta H_{\text{ITC}}^{\text{Cd}^{\text{II}}} - \Delta H_{\text{ITC}}^{\text{Zn}^{\text{II}}}$ (Figure 10). The $0.9 \text{ kcal mol}^{-1}$ gap between these two values (the Zn^{II}-to-Cd^{II} swap enthalpy subtracted from the apo-to-holo metalation enthalpy difference) can be explained by the contribution of the folding enthalpy ($\Delta H_{\text{fold}}^{\circ}$), which our results prove to be different for Zn^{II} and Cd^{II} complexes with Rad50.^[72–74] During the swap event, the hook is already present as a folded dimer, and the energetic contribution of metal-ion-exchange-induced structural changes is too small to be observed directly through this type of ITC experiment; hence, the observable difference is mainly dictated by the enthalpy of the Cd–S bond formation. On the other hand, direct titration of the apo peptide with Zn^{II} or Cd^{II} includes contributions of M–S bond formation ($\Delta H_{\text{M-S}}^{\circ}$), Cys thiol group deprotonation ($n_{\text{H}}\Delta H_{\text{CysH}}^{\circ}$), protonation of HEPES ($n_{\text{H}}\Delta H_{\text{HEPES}}^{\circ}$), and protomer folding ($\Delta H_{\text{fold}}^{\circ}$) [Eqs. (3) and (4)].

$$\Delta H^{\text{ITC}} = \Delta H^{\circ} + n_{\text{H}}\Delta H_{\text{HEPES}}^{\circ} \quad (3)$$

$$\Delta H^{\circ} = \Delta H_{\text{M-S}}^{\circ} + \Delta H_{\text{fold}}^{\circ} + n_{\text{H}}\Delta H_{\text{CysH}}^{\circ} \quad (4)$$

Assuming that Cys deprotonation and HEPES protonation enthalpies are equal for both Zn^{II} and Cd^{II} titrations, the energetic outcomes of metal–sulfur bond formation and protomer folding have to be different.^[75] Taking the above into account, one may conclude that the energetic cost of Rad50 protomer folding and dimerization is in fact different for Zn^{II} and Cd^{II} and can be roughly estimated for Cd(Hk14)₂ by the following subtraction: $\Delta\Delta H_{\text{Cd}^{\text{II}}-\text{Zn}^{\text{II}}}^{\text{ITC}} - \Delta H_{\text{swap}}^{\text{ITC}}$, which equals $-0.9 \text{ kcal mol}^{-1}$. Moreover, the entropic contribution, derived from the Gibbs equation as $T\Delta S^{\circ}$, is slightly lower for Cd(Hk14)₂ than for Zn(Hk14)₂, with 23.13 and 23.94 kcal mol^{-1} , respectively, suggesting that Cd^{II} may induce alternative hook folding that manifests as an entropy loss (Figure S13, Supporting Information). These calculations demonstrate that the molecular basis of the Cd^{II} complexes' elevated stability originates from the higher enthalpic contribution of both Cd–S bond formation and Cd^{II}-induced protomer folding, compared with Zn^{II} complexes, therefore indicating that Zn(Hk)₂ and Cd(Hk)₂ present different structural arrangements.

To evaluate values of thermodynamic parameters obtained in this study, we aimed to compare them with published ITC data for 4Cys metal-binding sites. Although the literature lacks consistent thermodynamic data for this particular metal-binding site, as well as the Cys residue alone binding to Zn^{II} and Cd^{II} ions, we managed to find some values. Krizek et al. obtained $\Delta G_{\text{C}}^{\text{Cd}^{\text{II}}} = -1.9 \text{ kcal mol}^{-1}$ for consensus zinc finger CP1 with the 4Cys metal-binding motif.^[61] Another zinc finger with a 4Cys binding motif, XPA, showed lower Gibbs free energy of around -4 kcal mol^{-1} for Cd^{II} complexation.^[23] On the other hand, Zn₄MT3 from *Musa acuminata* titrated with Cd^{II} gave observable heats of around -3 kcal mol^{-1} .^[76] Although the pre-

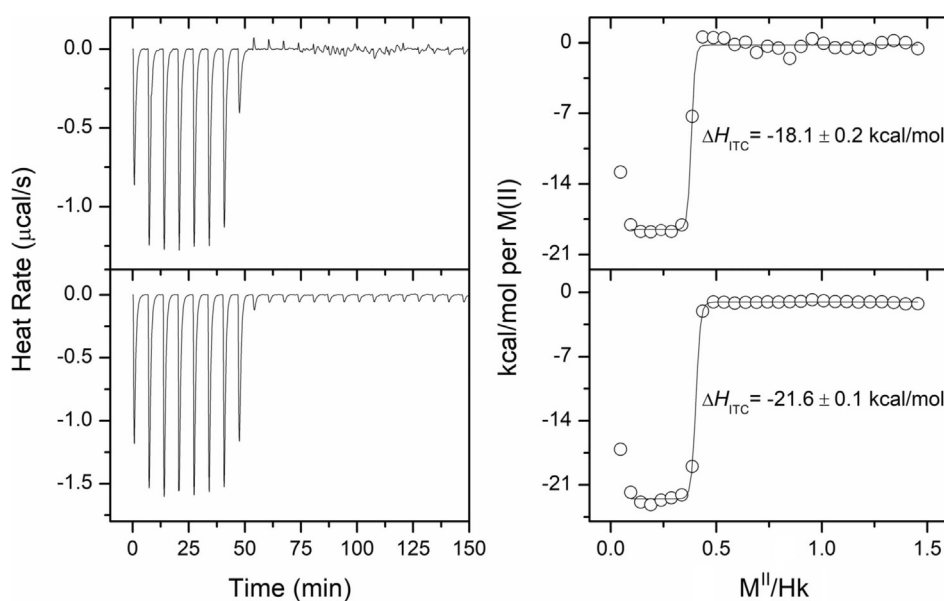


Figure 10. Isothermal titration calorimetry analysis of 100 μM Hk14 stepwise titrated with 650 μM ZnSO₄ (upper panel) or CdSO₄ (lower panel). Left graphs illustrate baseline-subtracted heat rate over time, and right graphs show observed enthalpy per mole of titrant (Zn^{II} or Cd^{II}) as a function of molar M^{II}-to-Hk14 ratio.

sented values seem to differ quite significantly, they are still comparable to our data, especially taking into account that none of the experiments were performed in exactly the same way, nor did they maintain high analytical standards. Nonetheless, the difference in Gibbs free energy values of Cd^{II} and Zn^{II} complexation by the Rad50 hook domain or other 4Cys binding motifs seems to vary at around -3 kcal mol^{-1} .

Biological significance

The Rad50 protein is an integral constituent of the MR(N/X) complex present in every living organism analyzed so far. MR as a heterotetrameric (or heterohexameric MR(N/X) in higher organisms) complex, comprised of two units of Mre11 nuclease and two units of Rad50, guards genomic integrity by sensing and repairing double-stranded DNA breaks that otherwise left unrepaired would cause deleterious genotoxic effects inevitably leading to cell death.^[27] Given that Mre11 is responsible for processing of the broken DNA ends, Rad50 plays a more structural role, acting as a lengthy scaffold for the complex and a major dimerization factor through action of the zinc hook domain located at the apex of the MR(N) complex. It is believed that the MR(N/X) complex is a flexible one with highly dynamic properties that enable it to adopt multiple conformational assemblies.^[26,28,29,31,77] Recent findings indicate that conformation-altering signals can be generated both at Rad50's ATPase globular and zinc hook domain apexes and transferred through an immensely long coiled-coil segment that spans 500 Å.^[34,35,43,45,77-79] At this point, two conformational states of the MR(N/X) complex seem to play a major functional role: closed conformation that binds tightly to DNA substrates and open conformation that enables DNA processing and repair.^[34,80] Both assemblies interact differently with DDR proteins and seem to be preferentially activated during different phases of the cell cycle.^[81,82] These data indicate that the zinc hook domain is much more than a simple dimerization motif and could possibly regulate the functional status of the entire complex. We have previously shown that any kind of amino-acid-substitution-based alterations render the zinc hook abrogated, destabilizing Zn^{II} binding in vitro and DNA damage repair in vivo.^[33,43] In this sense, any factor that inflicts structural changes upon the zinc hook domain has to be treated as a potential genotoxic agent.

Taking the above into account, Cd^{II} represents an evident threat to Rad50's functional status and therefore a threat to genomic integrity. Considering that Zn^{II}-binding proteins represent approximately 10% of the cell's proteome, Cd^{II}-swapping outcomes could be deleterious for multiple biochemical reasons. Intuitively, the most detrimental toxic effect pertains to DNA-binding proteins and transcription factors that ubiquitously harbor Zn^{II}-rich domains. Therefore, Rad50, with its zinc hook domain, poses as a perfect target for Cd^{II} toxicity.

Experimental results presented herein prove that Cd^{II} bound to Rad50 alters its structural status. The Cd(Rad50)₂ complex presents an augmented molecular volume that coincides with formation of extended helical regions, compared with Zn(Rad50)₂. Furthermore, the Cd^{II} ion is bound so tightly that it

renders the zinc hook domain effectively blocked in one rigid conformation and incapable of any Zn^{II}- or DDR-protein-driven structural rearrangements that seem to be crucial for the MR(N/X) complex's multifunctionality.

Conclusion

We hereby documented the most stable Cd^{II}-peptide complex described so far, with sub-zeptomolar affinity as a Cd(Rad50)₂ dimer, and determined molecular bases of Cd^{II}-induced stability elevation compared with its counterpart that naturally allocates in the Rad50 hook domain, that is, Zn^{II}. Cd^{II}, although similar to Zn^{II} in terms of physical properties, induces significant structural changes in the Rad50 hook domain. The reported increase in rotational correlation time and altered NMR spectroscopic structure suggest the possibility of Cd^{II}-binding-induced global MR(N/X) complex rearrangement, implying that this metal ion is capable of abrogating DNA-damage sensing and repair functions of the MR(N/X) complex in a cellular context. Additionally, the approximately two-orders-of-magnitude increase in Cd(Rad50)₂ stability compared with that of Zn(Rad50)₂ supports the notion that Cd^{II} is bound almost irreversibly to its target and renders it incapable of Zn^{II}- and DDR-factor-governed flexibility that seems to be crucial for proper double-stranded DNA damage repair. Our results show that this particular interaction of Cd^{II} may be one of the major reasons for its still-unresolved genotoxicity and show how Cd^{II} ions can impact intermolecular zinc-binding sites in oligomeric proteins.

Experimental Section

Materials

N,N-Diisopropylethylamine (DIEA), 9-fluorenylmethoxycarbonyl (Fmoc)-protected amino acids (Fmoc-Ala-OH·H₂O, Fmoc-Arg(Pbf)-OH, Fmoc-Asn(Trt)-OH, Fmoc-Asp(OtBu)-OH, Fmoc-Cys(Trt)-OH, Fmoc-Gln(Trt)-OH, Fmoc-Glu(OtBu)-OH, Fmoc-Gly-OH, Fmoc-His(Trt)-OH, Fmoc-Ile-OH, Fmoc-Leu-OH, Fmoc-Lys(Boc)-OH, Fmoc-Met-OH, Fmoc-Phe-OH, Fmoc-Pro-OH, Fmoc-Ser(tBu)-OH, Fmoc-Thr(tBu)-OH, Fmoc-Tyr(tBu)-OH, Fmoc-Val-OH), piperidine, *O*-(benzotriazol-1-yl)-*N,N,N,N'*-tetramethyluronium hexafluorophosphate (HBTU), and D,L-dithiothreitol (DTT) were purchased from Iris Biotech GmbH. Trifluoroacetic acid (TFA), 1,2-ethanedithiol (EDT), thioanisole, anisole, triisopropylsilane (TIPS), COMU, guanidine hydrochloride (GdnHCl), 4-mercaptophenylacetic acid, tris(2-carboxyethyl)phosphine hydrochloride (TCEP), ethylenediaminetetraacetic acid (EDTA), HCl (trace metal grade), bis(β-aminoethyl ether)-*N,N,N,N'*-tetraacetic acid (EGTA), *N*-carboxymethyl-*N'*-(2-hydroxyethyl)-*N,N'*-ethylenediglycine trisodium salt (Na₃-HEDTA), NaClO₄·H₂O, ZnSO₄·7H₂O, and CdSO₄·8/3H₂O were from Merck KGaA. Diethyl ether, acetic anhydride, dichloromethane (DCM), and NaCl were purchased from Avantor Performance Materials Poland S.A. Chelex 100 resin was from Bio-Rad, 4-(2-hydroxyethyl)piperazine-1-ethanesulfonic acid sodium salt (HEPES) was from Bioshop, 5,5'-dithiobis(2-nitrobenzoic acid) (DTNB) was from TCI Europe N.V., TentaGel R RAM and TentaGel S-NH₂ resins were from Rapp Polymere GmbH, and dimethylformamide (DMF) and acetonitrile (MeCN) were from VWR. All of the experiments were performed in che-

lexed buffers and solutions. All buffers were prepared with Milli-Q water obtained with a deionizing water system (Merck KGaA).

Peptide synthesis

Zinc hook peptides (Hk peptides) were synthesized by solid-phase peptide synthesis (SPPS) using an Fmoc-strategy on a TentaGel R RAM Amide Rink (Rapp Polymere GmbH, Tübingen, Germany) resin (substitution 0.2 mmol g^{-1}) and a Liberty 1 microwave-assisted synthesizer (CEM) as described previously.^[33,85] Peptides were N-terminally acetylated with acetic anhydride or fluorescently modified with a dansyl (Dns) moiety or 5(6)-carboxyfluorescein (FAM) derivatives. Cleaved peptides were precipitated and washed with cold diethyl ether and purified on a C18 column (Phenomenex) with a gradient of acetonitrile and 0.1% TFA using a Dionex Ultimate 3000 HPLC system. The identity of peptides was confirmed with an API 2000 Applied Biosystems ESI-MS instrument. Concentration of peptide stocks in 10 mM HCl was determined using a sulfhydryl-group reactant, DTNB ($\epsilon = 14,150 \text{ M}^{-1} \text{ cm}^{-1}$ at 412 nm), prior to each experiment.^[86]

Expression and purification of metal-free Hk130 and human metallothionein-2

The production of *P. furiosus* Hk130 and human metallothionein-2 (MT2) relied on a previously established protocol using the pTYB21 expression vector (IMPACT Protein Purification System, NEB) and *Escherichia coli* (*E. coli*) BL21-CodonPlus (DE3)-RIL strain.^[71] The expression vector is deposited in the Addgene plasmid repository (<https://www.addgene.org>), plasmid ID 105693 (MT2a). Transformed cells were cultivated in 4 L of LB or TB medium, respectively, and grown at 37 °C until OD_{600} was 0.4–0.5, and then induced with 0.1 mM IPTG. Cultures were incubated overnight at 20 °C with vigorous shaking and subsequently collected by centrifugation at $4500 \times g$ for 20 min at 4 °C. The pellets were resuspended in ice-cold buffer A (20 mM HEPES, pH 8.0, 500 mM NaCl, 1 mM EDTA, 1 mM TCEP) and lysed by sonication on ice for 30 min, followed by centrifugation at $20000 \times g$ for 15 min. Clarified cell extracts were incubated overnight with chitin resin at 4 °C with mild shaking. After the incubation, the resin was washed with 20 bed volumes of buffer A with increased salt concentration (1 M NaCl) to reduce nonspecific binding of other *E. coli* proteins. To induce the cleavage reaction, 25 mL of buffer B (20 mM HEPES, pH 8.0, 500 mM NaCl, 1 mM EDTA, 100 mM DTT) was added to the resin, and the mixture was incubated for 36–48 h at room temperature with mild shaking. Eluted protein solutions were acidified to $\text{pH} \approx 2.5$ –3.0 with 7% HCl and concentrated to a small volume using Amicon Ultra-4 Centrifugal Filter Units with NMWL of 3 kDa (Merck Millipore, USA). Hk130 protein was purified by reverse-phase HPLC in a 0.1% TFA/acetonitrile gradient (Dionex) followed by lyophilization, and MT2 was purified on an SEC-70 gel filtration column (Bio-Rad, USA) equilibrated with 5 mM HCl.^[70] The identity of metal-free MT2 and Hk130 protein was confirmed by ESI-MS, using an API 2000 instrument (Applied Biosystems, USA); the average molecular weight (MW) calculated was 6042.0/6042.2 Da (calcd/exp) and 15217.6/15217.8 Da (calcd/exp), respectively.

Reconstitution of cadmium metallothionein-2

To reconstitute the protein with Cd^{II} , aliquots of thionein in 5 mM HCl were mixed with cadmium sulfate at a molar ratio of 1:9 under a nitrogen blanket, and the pH adjusted to 8.6 with 1 M solution of Tris base and purified on an SEC-70 gel filtration column equilibrated with 20 mM Tris-HCl buffer, pH 8.6. The concentration of the pu-

rified protein was obtained spectrophotometrically, with DTNB and PAR assays for the thiol and Cd^{II} concentration, respectively.^[86,87] Additionally, samples were analyzed by inductively coupled plasma (ICP) analysis (ICP-AES iCAP 7400, Thermo Scientific) to confirm the spectrophotometric results.

Spectroscopic studies

The binding properties of hook peptides to Cd^{II} were examined by electronic absorption spectroscopy and circular dichroism by using a Cary 300 spectrophotometer (Varian) and Jasco J-1500 spectropolarimeter (Jasco) with a Peltier heating/cooling system, respectively. Spectra were recorded at 25 °C in the wavelength range of 200–280 nm to observe LMCT transitions^[39,85] as well as secondary structure changes.^[33] Three accumulations were averaged using a 5 nm band width, a 200 nm min^{-1} scanning speed, and a 1.0 nm data pitch. Depending on Hk length, 25–100 μM peptide in 20 mM Tris-HCl buffer (pH 7.4, $I = 0.1 \text{ M}$ from NaClO_4) was titrated with small aliquots of concentrated CdSO_4 to achieve molar ratios from 0 to 2 over Hk. After each addition of Cd^{II} , samples were equilibrated for 2–5 min and the spectra were recorded. All measurements were performed in the presence of fourfold excess of TCEP over Cys residue to avoid their oxidation. TCEP forms a very weak Cd^{II} complex ($\log K^{7.4} = 3.3$) compared with Hk peptides, and its metal-binding ability can be neglected.^[36] Zn^{II} -to- Cd^{II} replacement experiments were conducted on either equimolar or fivefold excess (to slow down the exchange) of Zn^{II} molar equivalent over Hk with Cd^{II} titration as described previously.

Potentiometry

The protonation constants of the Hk4–Hk14 zinc hook peptides and stability constants of their Cd^{II} complexes were determined at 25 °C at 0.1 M ionic strength (from KNO_3) by pH-metric titration over a range of 2.5 to 10.8, using a Molspin automatic titrator under argon with standardized 0.1 M NaOH as a titrant. The data were analyzed using SUPERQUAD software.^[49]

Fluorimetry and fluorescence anisotropy study

Fluorimetric studies were conducted with a Jobin Yvon Fluoromax-3 spectrofluorimeter (Horiba) equipped with a Peltier-thermostatted cell holder. Competition intra-FRET analysis was carried out as follows: 1 mM concentration of the appropriate Zn^{II} chelator (TPEN, EDTA, HEDTA) was used with various concentrations of ZnSO_4 (0.05–0.95 mM) in 50 mM HEPES, 100 mM NaCl, and 50 μM TCEP at pH 7.4 to maintain the free Zn^{II} concentration at a constant between subnano- and femtomolar levels. The concentration of zinc hook peptides in all studies was 5 μM . The sets of peptides in metal buffers (1.4 mL) were equilibrated over 48 h. Complex formation was measured by using FRET between Trp and Dns residues located at both ends of the zinc hook peptides. For that purpose, samples were excited at 290 nm, and spectra were collected in the range of 295–600 nm with a maximum emission of 543 nm. Anisotropy decay studies were performed with a DeltaFlex TCSPC Fluorimeter (Horiba) equipped with a Peltier-thermostatted cell holder. All measurements were carried out at 25 °C in the buffer described above with 500 nm N-terminally FAM-labeled hook peptides. FAM-labeled peptides (400 μL) were placed in a 1 mL all-transparent quartz cuvette and excited with a linearly polarized laser from DeltaDiode DD-485L (wavelength of 485 ± 10 nm) through a 2 nm slit. Emission data were detected at 521 nm wavelength with a sequentially changing polarizer from 0 to 90° until accumulation of 10000 peak difference at a 100 ns timescale was reached. Decay

data were subsequently fitted with DAS6 software using two- or three-exponential fitting, depending on the $-\log[M]_{\text{free}}$ and metal-to-peptide equilibrium, as a VV+VH sum, VV-VH difference, and anisotropy. Given the very small targets (Hk14-Hk45 peptides), only difference spectra from reconvolution anisotropy analyses were taken into account because this approach most precisely accounts for instrument-generated artifacts (Figures S14 and S15, Supporting Information). Zn^{II}-to-Cd^{II} exchange experiments carried out for Hk45 with equimolar content of Cd₂MT2a were performed accordingly, the only difference being faster equilibration times: 30 min for swap experiments and 36 h for competition experiments with metal chelators.

Competitive titrations

The apparent formation constants (K_{12}) of Cd^{II} biscomplexes with Hk14 and Hk45 peptides were determined fluorimetrically or spectropolarimetrically at 25 °C in the presence of Cd^{II} chelators HEDTA ($\log K^{7.4} = 12.2$), EDTA ($\log K^{7.4} = 13.6$), and TPEN ($\log K^{7.4} = 15.2$).^[56,60] In the case of fluorescently labeled peptides, 5 μM Hk was incubated with 1 mM chelator with various total Cd^{II} concentrations in HEPES buffer with 50 μM TCEP. For CD monitoring, 5 μM Hk peptide was incubated with 25 μM chelator and 0–22.5 μM ZnSO₄ in 20 mM Tris-HCl buffer (pH 7.4, $I = 0.1$ M from NaClO₄) with 100 μM TCEP. Samples were incubated for 36 h under nitrogen. The free Cd^{II} concentration present in each sample after equilibration was calculated from the total chelator and metal concentrations, corrected for the Cd^{II} transferred to the Hk peptide during Cd(Hk)₂ complex formation. Calculations were performed using the Hyperquad Simulation and Speciation Software (HySS2009).^[51] To obtain the apparent dissociation constants, we first determined the normalized isotherms corresponding to complex formation by fitting with Hill's equation.^[33] The obtained concentrations of free Cd^{II}, referring to the half-point complex saturation for which half of the total peptide is in the form of the Cd(Hk)₂ complex and half is in the metal-free form Hk, were subsequently used to calculate the apparent dissociation constants (K_{12}).

NMR spectroscopy

All spectra were measured with a DDR2 Agilent 600 MHz spectrometer equipped with a TRIAX probe. Assignment of ¹H and ¹³C signals (Table S2, Supporting Information) was based on the previously described assignment of a peptide complexed with Zn^{II}.^[33] 2D homonuclear TOCSY^[88] (mixing time 65 ms), NOESY^[89] (mixing time 150 ms), and heteronuclear ¹H-¹³C HSQC^[90] spectra recorded at 25 °C were used to confirm the assignment (relevant parameters of the NMR spectra are given in Table S3, Supporting Information). All chemical shifts in the ¹H NMR spectra are reported with respect to external sodium trimethylsilylpropanesulfonate ([D₄]DSS). Chemical shifts of the ¹³C spectra were referenced indirectly by using the 0.251449530 frequency ratios for ¹³C/¹H.^[91] Processed spectra were analyzed with SPARKY software.^[92]

Isothermal titration calorimetry

The binding of Cd^{II} and Zn^{II} to Hk peptides was monitored using a nano-ITC calorimeter (TA Waters, USA) at 25 °C with a cell volume of 1 mL. All experiments were performed in HEPES buffer ($I = 0.1$ M from NaCl) at pH 7.4 with 0.25 mM TCEP used as a non-metal-binding reducing agent.^[33,36] The Hk peptide (titrate) concentration was 0.1 mM, whereas the metal (titrant) concentration was 0.65 mM. After temperature equilibration, successive injections of the titrant were made into the reaction cell with 6.82 μL increments at 400 s

intervals with stirring at 200 rpm, with the exception of the Zn^{II}-to-Cd^{II} exchange experiment in which the titrant (CdSO₄) concentration was 1 mM and the injection volume was 4.83 μL . Control experiments to determine the heats of titrant dilution were performed using identical injections in the absence of Zn^{II} and Cd^{II}. The net reaction heat was obtained by subtracting the heat of dilution from the corresponding total heat of reaction. The titration data were analyzed using NanoAnalyze (version 3.3.0) and Origin (version 8.1) software.^[75]

Structure calculation

Determination of the structure of a symmetric dimer faces the well-known problem of ambiguity of restraints. In principle each NOE cross-peak can be a result of either contacts between protons of the same chain (intra) or different chains (inter) or both intra- and interchain contacts. Therefore, the structures of Hk14 peptide complexes with Cd^{II} and Zn^{II} ions were computed with Aria2 software,^[93] which can resolve ambiguous restraints in an iterative procedure. The parametrization of the coordination site with Zn^{II} ions was taken from the Aria2 program, with the exception of partial charges, which were computed using quantum chemistry methods applied to the model systems. For the complex with Cd^{II}, bond lengths between sulfur and cadmium (set to 2.636 Å) were set to average distances obtained from the crystal structure, and partial charges were adjusted to match those obtained from quantum chemistry computations. For both peptides, partial charges were manually corrected so that the total charge of the coordination site (ion and four cysteine residues) is equal to $-2|e|$. The procedure of structure calculation consisted of nine simulated annealing cycles followed by refinement in an explicit solvent of 10 with the lowest energy out of 300 structures obtained from the last simulated annealing cycle. Each simulated annealing cycle consisted of 45 ps of high temperature dynamics (2000 K) followed by two cooling cycles: 90 ps of cooling to 1000 K and 72 ps of cooling to 50 K. Finally, 200 steps of structure optimization with the Powell algorithm were applied. The problem of ambiguity of applied restraints (inter- or intramonomer) was solved by the iterative procedure of NOE assignment implemented in the Aria2 software. The C₂ symmetry of each complex was forced by application of special noncrystallographic symmetry restraints. Because of the ambiguity problem of NOE restraints, incorporation of additional hydrogen-bond restraints was necessary. For each complex, two types of structure determination procedures were applied. Both of them utilized NOE restraints and differed in the number of applied hydrogen-bond restraints. The first procedure (PROT) used hydrogen-bond information obtained from experimentally determined protection factors,^[33] whereas in the second procedure (CRYST) it was assumed that the same hydrogen bonds are formed as in the crystal structure (PDB code: 1L8D). All applied hydrogen-bond restraints are shown in Table S4. Notably, the CRYST method uses only one more hydrogen bond than the PROT method (backbone Gly3 O-Leu12 N). The average distance between two ends of the Hk14 peptide was estimated from 20 μs -long molecular dynamics simulation. The peptide in extended conformation was built with the xleap program from the AMBER18 suite.^[94] Interactions between atoms were described with the ff14SB force field.^[95] The peptide was immersed in a truncated octahedron box filled with TIP3P model explicit water molecules. The system was minimized, heated, and equilibrated in an NPT ensemble followed by a 20 μs -long NVT ensemble production run. The distance between ends was estimated as the average distance between α -carbon atoms of the first and last amino acid residue. For error estimation, the trajectory was divided into four 5 μs -long trajectories, and mean dis-

tances were calculated for each of them. The uncertainty was estimated as the standard deviation of mean values obtained from each window. Secondary structures were calculated for the whole trajectory with the DSSP method.^[96]

Acknowledgements

This research was financially supported by the National Science Centre (NCN) under Opus grant no. 2016/21/B/NZ1/02847 and Preludium grant no. 2016/23/N/NZ1/00040. The authors thank Anna Kocyla for her comments and editorial assistance.

Conflict of interest

The authors declare no conflict of interest.

Keywords: cadmium · DNA damage · Rad50 · zinc · zinc hook

- [1] D. Beyersmann, S. Hechtenberg, *Toxicol. Appl. Pharmacol.* **1997**, *144*, 247–261.
- [2] M. P. Waalkes, *Mutat. Res.* **2003**, *533*, 107–120.
- [3] M. Waisberg, P. Joseph, B. Hale, D. Beyersmann, *Toxicology* **2003**, *192*, 95–117.
- [4] P. Joseph, *Toxicol. Appl. Pharmacol.* **2009**, *238*, 272–279.
- [5] A. Hartwig, *Biometals* **2010**, *23*, 951–960.
- [6] A. Martelli, E. Rousselet, C. Dycke, A. Bouron, J. M. Moulis, *Biochimie* **2006**, *88*, 1807–1814.
- [7] D. H. Petering, *Chem. Res. Toxicol.* **2017**, *30*, 189–202.
- [8] I. Marszałek, W. Goch, W. Bal, *Inorg. Chem.* **2018**, *57*, 9826–9838.
- [9] R. A. Colvin, W. R. Holmes, C. P. Fontaine, W. Maret, *Metallomics* **2010**, *2*, 306–317.
- [10] W. Maret, J.-M. Moulis in *Cadmium: From Toxicity to Essentiality*, (Eds.: A. Sigel, H. Sigel, R. K. O. Sigel), Springer, Berlin, **2013**, Chapter 1, pp. 1–29.
- [11] D. R. Holland, A. C. Hausrath, D. Juers, B. W. Matthews, *Protein Sci.* **1995**, *4*, 1955–1965.
- [12] A. Hartwig, *Antioxid. Redox Signaling* **2001**, *3*, 625–634.
- [13] M. Vašák, G. E. Hawkes, J. K. Nicholson, P. J. Sadler, *Biochemistry* **1985**, *24*, 740–747.
- [14] M. Vašák, *Biodegradation* **1998**, *9*, 501–512.
- [15] M. J. Stillman, W. Cai, A. J. Zelazowski, *J. Biol. Chem.* **1987**, *262*, 4538–4548.
- [16] I. M. Armitage, T. Drakenberg, B. Reilly, *Met. Ions Life Sci.* **2013**, *11*, 117–144.
- [17] E. Freisinger, M. Vašák, *Met. Ions Life Sci.* **2013**, *11*, 339–371.
- [18] R. K. Kothinti, A. B. Blodgett, D. H. Petering, N. M. Tabatabai, *Toxicol. Appl. Pharmacol.* **2010**, *244*, 254–262.
- [19] G. Roesijadi, R. Bogumil, M. Vašák, J. H. Kägi, *J. Biol. Chem.* **1998**, *273*, 17425–17432.
- [20] G. Malgieri, L. Zaccaro, M. Leone, E. Bucci, S. Esposito, I. Baglivo, A. Del Gatto, L. Russo, R. Scandurra, P. V. Pedone, R. Fattorusso, C. Isernia, *Biopolymers* **2011**, *95*, 801–810.
- [21] G. Malgieri, M. Palmieri, S. Esposito, V. Maione, L. Russo, I. Baglivo, I. de Paola, D. Milardi, D. Diana, L. Zaccaro, P. V. Pedone, R. Fattorusso, C. Isernia, *Metallomics* **2014**, *6*, 96–104.
- [22] M. Asmuss, L. H. F. Mullenders, A. Eker, A. Hartwig, *Carcinogenesis* **2000**, *21*, 2097–2104.
- [23] E. Kopera, T. Schwerdtle, A. Hartwig, W. Bal, *Chem. Res. Toxicol.* **2004**, *17*, 1452–1458.
- [24] C. Méplan, K. Mann, P. Hainaut, *J. Biol. Chem.* **1999**, *274*, 31663–31670.
- [25] D. P. Giedroc, X. Chen, M. A. Pennella, A. C. Li Wang, *J. Biol. Chem.* **2001**, *276*, 42322–42332.
- [26] K. P. Hopfner, L. Craig, G. Moncalian, R. A. Zinkel, T. Usui, B. A. Owen, A. Karcher, B. Henderson, J. L. Bodmer, C. T. McMurray, J. P. Carney, J. H. J. Petrini, J. A. Tainer, *Nature* **2002**, *418*, 562–566.
- [27] T. H. Stracker, J. H. J. Petrini, *Nat. Rev. Mol. Cell. Biol.* **2011**, *12*, 90–103.
- [28] M. de Jager, J. van Noort, D. C. van Gent, C. Dekker, R. Kanaar, C. Wyman, *Mol. Cell* **2001**, *8*, 1129–1135.
- [29] F. Moreno-Herrero, M. de Jager, N. H. Dekker, R. Kanaar, C. Wyman, C. Dekker, *Nature* **2005**, *437*, 440–443.
- [30] Y. B. Park, M. Hohl, M. Padjasek, E. Jeong, K. S. Jin, A. Krężel, J. H. J. Petrini, Y. Cho, *Nat. Struct. Mol. Biol.* **2017**, *24*, 248–257.
- [31] K. Lammens, D. J. Bemeleit, C. Möckel, E. Clausing, A. Schele, S. Hartung, C. B. Schiller, M. Lucas, C. Angermüller, J. Söding, K. Strässer, K. P. Hopfner, *Cell* **2011**, *145*, 54–66.
- [32] T. Kochańczyk, P. Jakimowicz, A. Krężel, *Chem. Commun.* **2013**, *49*, 1312–1314.
- [33] T. Kochańczyk, M. Nowakowski, D. Wojewska, A. Kocyla, A. Ejchart, W. Koźmiński, A. Krężel, *Sci. Rep.* **2016**, *6*, 36346.
- [34] A. Syed, J. A. Tainer, *Annu. Rev. Biochem.* **2018**, *87*, 263.
- [35] E. Casari, C. Rinaldi, A. Marsella, M. Gnugnoli, C. V. Colombo, D. Bonetti, M. P. Longhese, *Front. Mol. Biosci.* **2019**, *6*, 43.
- [36] A. Krężel, R. Latajka, G. D. Bujacz, W. Bal, *Inorg. Chem.* **2003**, *42*, 1994–2003.
- [37] C. J. Henahan, D. L. Pountney, O. Zerbe, M. Vašák, *Protein Sci.* **1993**, *2*, 1756–1764.
- [38] A. Krężel, W. Leśniak, M. Jeżowska-Bojczuk, P. Młynarz, J. Brasuń, H. Kozłowski, W. Bal, *J. Inorg. Biochem.* **2001**, *84*, 77–88.
- [39] J. Adamczyk, W. Bal, A. Krężel, *Inorg. Chem.* **2015**, *54*, 596–606.
- [40] P. E. Eis, J. R. Lakowicz, *Biochemistry* **1993**, *32*, 7981–7993.
- [41] B. R. White, H. M. Liljestrand, J. A. Holcomb, *Analyst* **2008**, *133*, 65–70.
- [42] J. R. Lakowicz, *Principles of fluorescence spectroscopy*, Springer, Berlin, **2010**.
- [43] M. Hohl, T. Kochańczyk, C. Tous, A. Aguilera, A. Krężel, J. H. J. Petrini, *Mol. Cell* **2015**, *57*, 479–491.
- [44] J. J. Wiltzius, M. Hohl, J. C. Fleming, J. H. J. Petrini, *Nat. Struct. Mol. Biol.* **2005**, *12*, 403–407.
- [45] M. Hohl, Y. Kwon, S. M. Galván, X. Xue, C. Tous, A. Aguilera, P. Sung, J. H. J. Petrini, *Nat. Struct. Mol. Biol.* **2011**, *18*, 1124–1131.
- [46] M. A. Hink, R. A. Griep, J. W. Borst, A. van Hoek, M. H. M. Eppink, A. Schots, A. J. W. G. Visser, *J. Biol. Chem.* **2000**, *275*, 17556–17560.
- [47] A. Miłoch, A. Krężel, *Metallomics* **2014**, *6*, 2015–2024.
- [48] O. Sénèque, J. M. Latour, *J. Am. Chem. Soc.* **2010**, *132*, 17760–17774.
- [49] P. Gans, A. Sabatini, A. Vacca, *J. Chem. Soc. Dalton Trans.* **1985**, *6*, 1195–1200.
- [50] O. Sénèque, E. Bonnet, F. L. Joumas, J. M. Latour, *Chem. Eur. J.* **2009**, *15*, 4798–4810.
- [51] L. Alderighi, P. Gans, A. Ienco, D. Peters, A. Sabatini, A. Vacca, *Coord. Chem. Rev.* **1999**, *184*, 311–318.
- [52] A. Pomorski, T. Kochańczyk, A. Miłoch, A. Krężel, *Anal. Chem.* **2013**, *85*, 11479–11486.
- [53] K. Kluska, J. Adamczyk, A. Krężel, *Coord. Chem. Rev.* **2018**, *367*, 18–64.
- [54] A. Kocyla, J. Adamczyk, A. Krężel, *Metallomics* **2018**, *10*, 120–131.
- [55] A. Krężel, J. Wójcik, M. Maciejczyk, W. Bal, *Chem. Commun.* **2003**, *6*, 704–705.
- [56] A. Krężel, W. Maret, *Arch. Biochem. Biophys.* **2016**, *611*, 3–19.
- [57] L. S. Busenlehner, N. J. Cospser, R. A. Scott, B. P. Rosen, M. D. Wong, D. P. Giedroc, *Biochemistry* **2001**, *40*, 4426–4436.
- [58] Y. Wang, L. Hemmingsen, D. P. Giedroc, *Biochemistry* **2005**, *44*, 8976–8988.
- [59] Y. Wang, E. A. Mackay, M. Kurasaki, J. H. R. Kägi, *Eur. J. Biochem.* **1994**, *225*, 449–457.
- [60] A. E. Martell, R. M. Smith, *Critical Stability Constants*, Plenum Press, New York, **1974**.
- [61] B. A. Krizek, D. L. Merkle, J. M. Berg, *Inorg. Chem.* **1993**, *32*, 937–940.
- [62] G. Galbács, H. Szokolai, A. Kormányos, A. Metzinger, L. Szekeres, C. Marcu, F. Peter, C. Muntean, A. Negrea, M. Ciopec, A. Jancsó, *Bull. Chem. Soc. Jpn.* **2016**, *89*, 243–253.
- [63] M. Rowińska-Żyrek, D. Witkowska, S. Bielińska, W. Kamysz, H. Kozłowski, *Dalton Trans.* **2011**, *40*, 5604–5610.
- [64] M. Margoshes, B. L. Vallee, *J. Am. Chem. Soc.* **1957**, *79*, 4813–4814.
- [65] M. Vašák, G. Meloni, *J. Biol. Inorg. Chem.* **2011**, *16*, 1067–1078.
- [66] K. Honda, R. Tatsukawa, *R. Arch. Environ. Contam. Toxicol.* **1983**, *12*, 543–550.
- [67] K. A. Melis, D. C. Carter, C. D. Stout, D. R. Winge, *J. Biol. Chem.* **1983**, *258*, 6255–6257.

- [68] A. H. Robbins, D. E. McRee, M. Williamson, S. A. Collett, N. H. Xuong, W. F. Furey, B. C. Wang, C. D. Stout, *J. Mol. Biol.* **1991**, *221*, 1269–1293.
- [69] A. Krężel, W. Maret, *Int. J. Mol. Sci.* **2017**, *18*, E1237.
- [70] A. Krężel, W. Maret, *J. Am. Chem. Soc.* **2007**, *129*, 10911–10921.
- [71] A. Droz, D. Wojewska, M. D. Peris-Díaz, P. Jakimowicz, A. Krężel, *Metalomics* **2018**, *10*, 595–613.
- [72] A. M. Rich, E. Bombarda, A. D. Schenk, P. E. Lee, E. H. Cox, A. M. Spuches, L. D. Hudson, B. Kieffer, D. E. Wilcox, *J. Am. Chem. Soc.* **2012**, *134*, 10405–10418.
- [73] C. A. Blasie, J. M. Berg, *Biochemistry* **2002**, *41*, 15068–15073.
- [74] A. R. Reddi, T. R. Guzman, R. M. Breece, D. L. Tierney, B. R. Gibney, *J. Am. Chem. Soc.* **2007**, *129*, 12815–12827.
- [75] C. F. Quinn, M. C. Carpenter, M. L. Croteau, D. E. Wilcox, *Methods Enzymol.* **2016**, *567*, 3–21.
- [76] A. C. S. Cabral, J. Jakovleska, A. Deb, J. E. Penner-Hahn, V. L. Pecoraro, E. Freisinger, *J. Biol. Inorg. Chem.* **2018**, *23*, 91–107.
- [77] R. A. Deshpande, G. J. Williams, O. Limbo, R. S. Williams, J. Kuhnlein, J. H. Lee, S. Classen, G. Guenther, P. Russell, J. A. Tainer, T. T. Paull, *EMBO J.* **2014**, *33*, 482–500.
- [78] J. H. Lee, M. R. Mand, R. A. Deshpande, E. Kinoshita, S. H. Yang, C. Wyman, T. T. Paull, *J. Biol. Chem.* **2013**, *288*, 12840–12851.
- [79] J. Lafrance-Vanasse, G. J. Williams, J. A. Tainer, *Prog. Biophys. Mol. Biol.* **2015**, *117*, 182–193.
- [80] T. T. Paull, A. R. Deshpande, *Exp. Cell Res.* **2014**, *329*, 139–147.
- [81] Y. Aylon, B. Liefshitz, M. Kupiec, *EMBO J.* **2004**, *23*, 4868–4875.
- [82] X. Chen, H. Niu, W. H. Chung, Z. Zhu, A. Papusha, E. Y. Shim, S. E. Lee, P. Sung, G. Ira, *Nat. Struct. Mol. Biol.* **2011**, *18*, 1015–1019.
- [83] V. Dorcak, A. Krężel, *Dalton Trans.* **2003**, 2253–2259.
- [84] J. L. Michalek, S. J. Lee, S. L. J. Michel, *J. Inorg. Biochem.* **2012**, *112*, 32–38.
- [85] K. Kluska, J. Adamczyk, A. Krężel, *Metalomics* **2018**, *10*, 248–263.
- [86] P. Eyer, F. Worek, D. Kiderlen, G. Sinko, A. Stuglin, V. Simeon-Rudolf, E. Reiner, *Anal. Biochem.* **2003**, *312*, 224–227.
- [87] A. Kocyla, A. Pomorski, A. Krężel, *J. Inorg. Biochem.* **2015**, *152*, 82–89.
- [88] L. Braunschweiler, R. R. Ernst, *J. Magn. Reson. (1969–1992)* **1983**, *53*, 521–528.
- [89] J. Jeener, P. Bachmann, R. R. Ernst, *J. Chem. Phys.* **1979**, *71*, 4546–4553.
- [90] G. Bodenhausen, D. J. Ruben, *Chem. Phys. Lett.* **1980**, *69*, 185–189.
- [91] D. S. Wishart, C. G. Bigam, A. Holm, R. S. Hodges, B. D. Sykes, *J. Biomol. NMR* **1995**, *5*, 67–81.
- [92] SPARKY 3, T. D. Goddard, D. G. Kneller, University of California, San Francisco, **2000**.
- [93] W. Rieping, M. Habeck, B. Bardiaux, A. Bernard, T. E. Malliavin, M. Nilges, *Bioinformatics* **2007**, *23*, 381–382.
- [94] AMBER 2018, D. A. Case, I. Y. Ben-Shalom, S. R. Brozell, D. S. Cerutti, T. E. Cheatham III, V. W. D. Cruzeiro, T. A. Darden, R. E. Duke, D. Ghoreishi, M. K. Gilson, H. Gohlke, A. W. Goetz, D. Greene, R. Harris, N. Homeyer, Y. Huang, S. Izadi, A. Kovalenko, T. Kurtzman, T. S. Lee, S. LeGrand, P. Li, C. Lin, J. Liu, T. Luchko, R. Luo, D. J. Mermelstein, K. M. Merz, Y. Miao, G. Monard, C. Nguyen, H. Nguyen, I. Omelyan, A. Onufriev, F. Pan, R. Qi, D. R. Roe, A. Roitberg, C. Sagui, S. Schott-Verdugo, J. Shen, C. L. Simmerling, J. Smith, R. Salomon-Ferrer, J. Swails, R. C. Walker, J. Wang, H. Wei, R. M. Wolf, X. Wu, L. Xiao, D. M. York, P. A. Kollman, University of California, San Francisco, **2018**.
- [95] J. A. Maier, C. Martinez, K. Kasavajhala, L. Wickstrom, K. E. Hauser, C. Simmerling, *J. Chem. Theory Comput.* **2015**, *11*, 3696–3713.
- [96] W. Kabsch, C. Sander, *Biopolymers* **1983**, *22*, 2577–2637.

Manuscript received: October 29, 2019

Revised manuscript received: December 12, 2019

Accepted manuscript online: December 17, 2019

Version of record online: January 30, 2020